Journal of Catalysis **199,** 177–192 (2001)
doi:10.1006/jcat.2001.3161, available online at http://www.idealibrary.com on IDEAL®

$SrCl_2$-Promoted REO_x (RE = Ce, Pr, Tb) Catalysts for the Selective Oxidation of Ethane: A Study on Performance and Defect Structures for Ethene Formation

H. X. Dai, C. F. Ng, and C. T. Au[1]

Department of Chemistry and Center for Surface Analysis and Research, Hong Kong Baptist University, Kowloon Tong, Hong Kong

Received June 30, 2000; revised January 4, 2001; accepted January 4, 2001; published online March 27, 2001

The performance and characterization of the $SrCl_2$-promoted REO_x (RE = Ce, Pr, Tb) catalysts have been investigated for the oxidative dehydrogenation of ethane (ODE) reaction. The doping of $SrCl_2$ to REO_x significantly reduced C_2H_4 deep oxidation and enhanced C_2H_4 selectivity and C_2H_6 conversion. It has been shown that the catalytic performance increases in the order of 30 mol% $SrCl_2/CeO_2$ < 30 mol% $SrCl_2/PrO_{1.83}$ < 40 mol% $SrCl_2/TbO_{1.75}$. We observed that Cl leaching was modest in the latter two catalysts but gradual Cl loss was observed over the first catalyst. Within a reaction period of 60 h, the first catalyst degraded, whereas the latter two catalysts were stable. The C_2H_6 conversion, C_2H_4 selectivity, and C_2H_4 yield measured 1 h after the start of the ODE reaction were, respectively, 72.6, 68.8, and 49.9% for 30 mol% $SrCl_2/CeO_2$, 79.1, 71.4, and 56.5% for 30 mol% $SrCl_2/PrO_{1.83}$, and 82.6, 75.8, and 62.6% for 40 mol% $SrCl_2/TbO_{1.75}$ at 660°C and 1.67 × 10^{-4} h g mL^{-1} contact time. The results of X-ray photoelectron spectroscopy (XPS) and chemical analyses of chloride indicated that Cl^- ions were uniformly distributed in 30 mol% $SrCl_2/PrO_{1.83}$ and 40 mol% $SrCl_2/TbO_{1.75}$, but were not so in 30 mol% $SrCl_2/CeO_2$. The Ce 3*d*, Pr 3*d*, and Tb 4*d* spectra obtained in XPS studies demonstrated that there are RE^{3+} and RE^{4+} ions present in the $SrCl_2$-doped catalysts and $SrCl_2$ doping facilitates the redox cycle of the RE^{3+}/RE^{4+} couple via RE^{3+} generation. The results of O_2 temperature-programmed desorption (TPD) studies showed that the addition of $SrCl_2$ to REO_x could obviously lower the desorption temperature of lattice oxygen. Temperature-programmed reduction (TPR) results revealed that $SrCl_2$ doping causes the reduction temperatures of lattice O^{2-} in REO_x to decrease; in other words, the activity of lattice O^{2-} was promoted. We consider that such behaviors are closely associated with the defect structures formed in ionic exchanges between the $SrCl_2$ and the REO_x phases. X-ray diffraction (XRD) results indicated that, among the three $SrCl_2$-doped catalysts, 40 mol% $SrCl_2/TbO_{1.75}$ showed a cubic $TbO_{1.75}$ lattice most significantly enlarged and a $SrCl_2$ lattice most pronouncedly shrunk. *In situ* laser Raman results indicated that there were dioxygen adspecies such as O_2^{2-} and O_2^- on the 30 mol% $SrCl_2/CeO_2$ catalyst. XPS results indicated that there were O^-, O_2^{2-}, and/or O_2^- species on REO_x, 30 mol% $SrCl_2/CeO_2$, 30 mol% $SrCl_2/PrO_{1.83}$, and 40 mol% $SrCl_2/PrO_{1.75}$. On the basis of the results of *in situ* Raman, O_2-TPD, TPR, $^{18}O_2$- and C_2H_6-pulsing, and XPS studies, we suggest that O_2^{2-} and O_2^- as well as surface lattice O^{2-} species participate in the selective oxidation of ethane to ethene, whereas in excessive amount, the O^- species tend to induce the deep oxidation of ethane. © 2001 Academic Press

Key Words: **multivalent lanthanide oxides; $SrCl_2$-promoted REO_x (RE = Ce, Pr, Tb) catalysts; selective oxidation; ethane oxidative dehydrogenation; lattice oxygen activity; XPS characterization.**

INTRODUCTION

Since the pioneering work of Keller and Bhasin in 1982 (1) there have been numerous reports on the oxidative coupling of methane (OCM) to C_{2+} hydrocarbons and the oxidative dehydrogenation of ethane (ODE) reactions. Many catalysts, such as transition metal (Mo, V, Nb, Ti, Cr, Mn, Fe, Co, Ni, and Ta) oxides (2–5), alkali metal (Li, Na, K, and Cs)-doped magnesium oxides (6–11), perovskite-type oxides (12, 13), layered compound $KSr_2Bi_3O_4Cl_6$ (14), LiCl-promoted ZrO_2 (15), Nd_2O_3-doped LiCl/sulfated ZrO_2 (16), rare earth oxides (17–19), Li/Ca/La_2O_3 (20), and halide-modified rare earth oxides or oxyhalides (21–30), have been developed. For the ODE reaction, the Mo–V–Nb–Sb–Ca–O (5) and Dy_2O_3/Li^+–MgO–Cl^- (10) catalysts give a 73–75% C_2H_6 conversion and a 71–76% C_2H_4 selectivity at relatively lower temperatures (400–570°C), the 5 wt% Nd_2O_3–5 wt% LiCl/sulfated ZrO_2 catalyst (16) gives a ca. 93% C_2H_6 conversion and a ca. 83% C_2H_4 selectivity at 650°C, whereas the Li/Ca/La_2O_3 (20) and 50 mol% LaF_3/CeO_2 (21) catalysts show a ca. 93% C_2H_4 selectivity and a 23–47% C_2H_6 conversion at higher temperatures (650–670°C).

Over transition metal (with at least two different oxidation states) oxides, the ODE reaction proceeds via a redox cycle of metal ions, and the metal ion couples (with higher and lower oxidation states) actually function as active centers. In the ODE reaction, O_2 molecules receive electrons that are released from the metal ions with lower valence

[1] To whom correspondence should be addressed. Fax: (852) 2339-7348. E-mail: pctau@hkbu.edu.hk.

0021-9517/01 $35.00

state and transform into lattice oxygen before being involved in the ODE reaction (4). Over nonreducible metal oxide catalysts, the ODE reaction is undergone via the interaction of C_2H_6 with activated oxygen species; the nature and concentrations of surface oxygen species have a direct influence on the catalytic performance of such catalysts (22–26). Generally speaking, O_2 can be activated on solid materials rich in lattice defects such as oxygen vacancies, trapped electrons, and charge-deficient oxygen. Nonreducible rare earth oxides harbor few lattice defects. Adding alkali metal (oxidation state, +1) or alkaline earth metal (oxidation state, +2) oxides or halides to rare earth (oxidation state, +3) oxides or oxyhalides, however, could generate lattice deformation by partial ionic exchanges, creating defect structures favorable for the activation of O_2 (21–37). Halogen in a catalyst has generally been believed to have positive effects on the OCM and ODE reactions. In terms of promoting rare earth oxide catalytic behavior, halide doping could significantly enhance the C_2H_6 conversion and C_2H_4 selectivity in the ODE reaction (21–26) and the introduction of chloride ions to some catalysts could prevent CO_2 poisoning and lower the reactivity of oxygen adspecies (7, 25). In the past decades, much attention has been paid to the identification and functions of oxygen adspecies. Activated oxygen usually exists in the form of dioxygen [O_2^{2-}, O_2^{n-} $(1 < n < 2)$, O_2^-, and $O_2^{\delta-}$ $(0 < \delta < 1)$] or monooxygen (O^-). Although O^- has been reported to be active for the OCM reaction (38), most researchers believe that dioxygen species are active for selective oxidation (22–27, 39–41), whereas O^- is prone to induce deep oxidation (25, 26, 42). Unlike the stoichiometric lanthanide sesquioxides, the REO_x ($RE =$ Ce, Pr, Tb) oxides exhibit multiple accessible cationic oxidation states (usually +3 and +4). The interconversion of oxidation states between +3 and +4 involves the release or storage of oxygen. The extremely mobile lattice oxygen in the REO_x could participate in the oxidation reaction of hydrocarbons (43). Kennedy and Cant (18) pointed out that in the ODE reaction, the specific mass activity of $PrO_{1.83}$ was higher than that of CeO_2; the C_2H_4 selectivity at 750°C decreased in the order of La_2O_3 (74.0%) > Sm_2O_3 (68.0%) > CeO_2 (57.0%) > $PrO_{1.83}$ (53.0%). Although single-component CeO_2 (44, 45), $PrO_{1.83}$ (35), and $TbO_{1.75}$ (44, 45) gave poor selectivities to C_{2+} compounds in the OCM reaction, the addition of alkali metal compounds (35–37) or alkaline earth fluorides (46–49) to these multivalent rare earth oxides could significantly enhance the C_{2+} product selectivities.

In recent years, our group has been looking for a good combination of alkaline earth metal halides and rare earth oxides or oxyhalides for the OCM and ODE reactions. Although MX_2 ($M =$ Sr, Ba; $X =$ F, Cl, Br)/Ln_2O_3 ($Ln =$ La, Nd, Sm, Ho, Y) show good initial catalytic activities, most of them deteriorate gradually due to halogen leaching (24–30). Only the 30 mol% $BaCl_2/Y_2O_3$ (25), 40 mol% $SrCl_2/Sm_2O_3$ (26), and 40 mol% $SrCl_2/Nd_2O_3$ (26) catalysts were found to be stable within 40 or 60 h of onstream ODE reaction. According to our published and unpublished results, the promotional effect of MX_2 on Ln_2O_3 generally follows the sequence of $SrCl_2$, $BaCl_2 > SrBr_2$, $BaBr_2 > SrF_2$, BaF_2. Both $SrCl_2$ and $BaCl_2$ are good dopants of the rare earth oxides that show a stable oxidation state of +3. In modifying variable-valence rare earth oxides for the ODE reaction, we observed that $SrCl_2$ had a better promotional effect on REO_x ($RE =$ Ce, Pr, Tb) than barium or other strontium halides. In the present study, we report the catalytic properties of the $SrCl_2$-promoted REO_x ($RE =$ Ce, Pr, Tb) catalysts and used techniques such as X-ray diffraction (XRD), X-ray photoelectron spectroscopy (XPS), O_2 temperature-programmed desorption (TPD), temperature-programmed reduction (TPR), $^{18}O_2$- and C_2H_6-pulsing, and *in situ* Raman Spectroscopy to characterize these catalytic materials.

EXPERIMENTAL

The $SrCl_2/REO_x$ ($RE =$ Ce, Pr, Tb) catalysts were prepared by wet-impregnation of CeO_2, $PrO_{1.83}$ (Pr_6O_{11}), and $TbO_{1.75}$ (Tb_4O_7) (Aldrich, >99.9%) powders, respectively, with an aqueous solution of $SrCl_2$ (Aldrich, >99.9%) at the desired molar ratios. After evaporation, the resulting pastes were dried at 120°C overnight and calcined at 900°C for 24 h and then in turn ground, pressed, crushed, and sieved into 80–100 mesh.

Catalytic measurements were performed according to the previously described procedures (25). C_2H_6 conversion and C_2H_4, CH_4, CO, and CO_2 selectivities were calculated on the basis of the balance of carbon (22). The balances of carbon and oxygen were estimated to be 100 ± 2 and $100 \pm 3\%$, respectively, for every run over the catalysts.

The crystal phases of the catalysts were determined on an XRD apparatus (D-MAX, Rigaku Rotaflex) operating at 40 kV and 100 mA using Cu$K\alpha$ radiation. The XPS (Leybold Heraeus-Shengyang SKL-12, VG CLAM 4 MCD Analyser) technique with Mg$K\alpha$ ($h\nu = 1253.6$ eV) as the excitation source was used to determine the O 1*s*, Ce 3*d*, Pr 3*d*, and Tb 4*d* binding energies of surface oxygen, cerium, praseodymium, and terbium species as well as to evaluate the surface chlorine compositions of the samples. The instrumental resolution is 0.5 eV. Before XPS measurements, the samples were calcined in O_2 (flow rate, 20 mL min^{-1}) at 800°C for 1 h and then cooled in O_2 to room temperature, followed by He (20 mL min^{-1}) treatment for 10 min at room temperature or further treatments in H_2 (20 mL min^{-1}) at the desired temperatures for 10 min and then cooled in He (20 mL min^{-1}) to room temperature. After outgassing in the primary vacuum chamber (10^{-5} Torr) for 0.5 h, the treated samples were then introduced into the ultrahigh-vacuum chamber (3×10^{-9} Torr) for recording. The C 1*s*

line at 284.6 eV was taken as a reference for binding energy calibration. The surface chlorine contents in the catalysts were calculated according to the approach described in Ref. (30). The specific surface areas of the catalysts were measured using a Nova 1200 apparatus and calculated according to the BET method. The halogen contents were analyzed according to the procedures reported in Ref. (30).

Pulse experiments were performed to investigate the reactivity of surface oxygen species. A catalyst sample (0.2 g) was placed in a microreactor and was thermally treated at a desired temperature for 15 min before the pulsing of $^{18}O_2$ or C_2H_6 and the effluent was analyzed online by a mass spectrometer. In order to confirm the involvement of surface lattice oxygen in the ODE reaction, we treated the sample at a desired temperature in He (flow rate, 20 mL min^{-1}) for 1 h and then kept on pulsing $^{18}O_2$ at a lower temperature until no observable change in the pulse size was detected. After purging the sample with He for 0.5 h, we pulsed C_2H_6 onto the treated sample and analyzed the effluent compositions. The pulse size was 65.7 μL (at 25°C, 1 atm) and He (HKO, purity >99.995%) was the carrier gas.

In situ laser Raman experiments were conducted using a Nicolet 560 FT Raman spectrometer. The samples were treated in O_2, H_2, or $C_2H_6/O_2/N_2$ (molar ratio = 2/1/3.7) at different temperatures. After various treatments, the samples were monitored at 25°C without being exposed to air.

The O_2-TPD and TPR experiments were performed according to the methods described in Ref. (25). The temperature range was from room temperature to 900°C. The temperature ramp was 10°C min^{-1}. The amount of O_2 desorbed from the catalysts was quantified by calibrating the peak areas against that of a standard pulse.

RESULTS

Catalytic Performance

Table 1 shows the catalytic performance of REO_x, $SrCl_2$, 30 mol% $SrCl_2/CeO_2$, 30 mol% $SrCl_2/PrO_{1.83}$, and 40 mol% $SrCl_2/TbO_{1.75}$ after 1 h of reaction at 660°C and 1.67×10^{-4} h g mL^{-1}. One can observe that quartz sand and $SrCl_2$ showed poor activities below 680°C. The undoped REO_x gave 32–41% C_2H_6 conversion, 25–36% C_2H_4 selectivity, and 9–15% C_2H_4 yield. With the doping of $SrCl_2$, there were significant increases in C_2H_6 conversions, C_2H_4 selectivities, and C_2H_4 yields. Among the three $SrCl_2$-modified catalysts, 40 mol% $SrCl_2/TbO_{1.75}$ performed the best, giving 82.6% C_2H_6 conversion, 75.8% C_2H_4 selectivity, and 62.6% C_2H_4 yield.

Figure 1 shows the catalytic performance of 30 mol% $SrCl_2/CeO_2$, 30 mol% $SrCl_2/PrO_{1.83}$, and 40 mol% $SrCl_2/TbO_{1.75}$ as a function of reaction temperature at 1.67×10^{-4} h g mL^{-1}. With the rise in temperature from 540 to 680°C, conversions of C_2H_6 and O_2 and selectivities of C_2H_4 and CH_4 increased over the three catalysts. Over 30 mol% $SrCl_2/CeO_2$, C_2H_4 selectivity first increased and then decreased; the highest C_2H_4 yield of 49.9% was achieved at 660°C where C_2H_6 and O_2 conversions and C_2H_4 selectivity were 72.6, 89.1, and 68.8%, respectively. Over the 30 mol% $SrCl_2/PrO_{1.83}$ and 40 mol% $SrCl_2/TbO_{1.75}$ catalysts, C_2H_4 selectivities and C_2H_4 yields first increased and then declined; for 30 mol% $SrCl_2/PrO_{1.83}$ the highest C_2H_4 yield was 56.5% at 660°C, with C_2H_6 and O_2 conversions and C_2H_4 selectivity being 79.1, 92.6, and 71.4%, respectively; for 40 mol% $SrCl_2/TbO_{1.75}$ it was 62.6%, with the corresponding C_2H_6 and O_2 conversions and C_2H_4 selectivity being 82.6, 93.3, and 75.8%.

The catalytic performance of $SrCl_2/CeO_2$, $SrCl_2/PrO_{1.83}$, and $SrCl_2/TbO_{1.75}$ versus $SrCl_2$ loading at 660°C and 1.67×10^{-4} h g mL^{-1} is shown in Fig. 2. Over the three catalysts, with the increase in $SrCl_2$ loading, C_2H_4 and CH_4 selectivities increased, whereas O_2 conversions and CO_x selectivities decreased; C_2H_6 conversions and C_2H_4 yields first increased and then decreased. The maximal C_2H_4 yield was, respectively, 49.9% for 30 mol% $SrCl_2/CeO_2$ (Fig. 2a), 56.5% for 30 mol% $SrCl_2/PrO_{1.83}$ (Fig. 2b), and 62.6% for 40 mol% $SrCl_2/TbO_{1.75}$ (Fig. 2c).

TABLE 1

Catalytic Performance after an Onstream Time of 1 h over REO_x, 30 mol% $SrCl_2/CeO_2$, 30 mol% $SrCl_2/PrO_{1.83}$, and 40 mol% $SrCl_2/TbO_{1.75}$ at 660°C and 1.67×10^{-4} h g mL^{-1}

Catalyst	Conversion (%)		Selectivity (%)				Yield (%)	Rate of C_2H_6 reaction
	C_2H_6	O_2	CO	CO_2	CH_4	C_2H_4	C_2H_4	(10^{18} molecules m^{-2} s^{-1})
Quartz sand[a]	7.6	—	0.9	9.9	0	89.2	6.8	—
CeO_2	31.6	100	0	69.8	0	30.2	9.5	0.153
$PrO_{1.83}$	35.4	100	0	75.4	0	24.6	8.7	0.164
$TbO_{1.75}$	41.2	100	0	63.6	0	36.4	15.0	0.264
$SrCl_2$	2.0	11.1	1.1	10.2	0.1	88.6	1.8	—
$SrCl_2/CeO_2$	72.6	89.1	3.3	27.0	0.9	68.8	49.9	0.437
$SrCl_2/PrO_{1.83}$	79.1	92.6	3.2	24.1	1.3	71.4	56.5	0.450
$SrCl_2/TbO_{1.75}$	82.6	93.3	4.3	17.9	2.0	75.8	62.6	0.566

[a] Tested at 680°C.

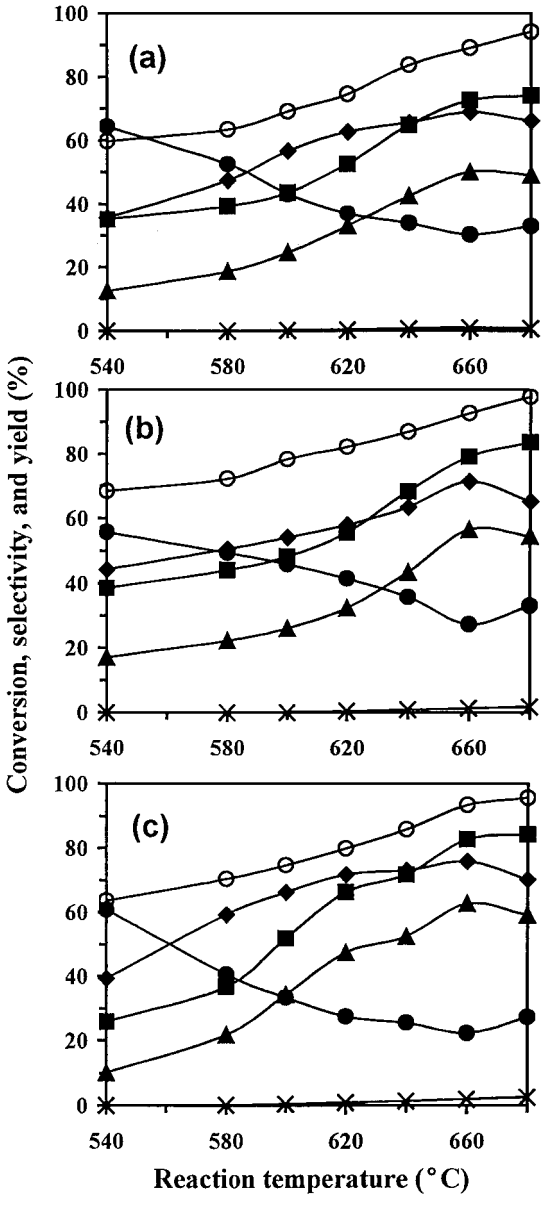

FIG. 1. Catalytic performance of (a) 30 mol% $SrCl_2/CeCO_2$, (b) 30 mol% $SrCl_2/PrO_{1.83}$, and (c) 40 mol% $SrCl_2/TbO_{1.75}$ as a function of reaction temperature at 1.67×10^{-4} h g ml^{-1}: (■) C_2H_6 conversion, (◆) C_2H_4 selectivity, (▲) C_2H_4 yield, (×) CH_4 selectivity, and (●) CO_x selectivity.

Table 2 summarizes the results of C_2H_4 and C_2H_6 oxidation, respectively, over the REO_x, 30 mol% $SrCl_2/CeO_2$, 30 mol% $SrCl_2/PrO_{1.83}$, and 40 mol% $SrCl_2/TbO_{1.75}$ catalysts at 660°C and 1.67×10^{-4} h g mL^{-1}. With the addition of $SrCl_2$ to REO_x, C_2H_4 selectivity increased in the ODE reaction, whereas C_2H_4 conversion decreased significantly in the ethene oxidation reaction. Furthermore, the CO/CO_2 ratios in the product mixture obtained over the $SrCl_2$-modified catalysts were much higher than those obtained over the single-component oxide catalysts. It is apparent that the presence of halide ions can noticeably reduce C_2H_4 deep oxidation.

Figure 3 shows the catalytic performance of 30 mol% $SrCl_2/CeO_2$, 30 mol% $SrCl_2/PrO_{1.83}$, and 40 mol% $SrCl_2/TbO_{1.75}$ during 60 h of onstream reaction at 660°C and 1.67×10^{-4} h g mL^{-1}. It is observed that the first catalyst decreased by ca. 15% in C_2H_6 conversion, ca. 11% in C_2H_4 selectivity, and ca. 17% C_2H_4 yield after 60 h, whereas the other two catalysts exhibited stable behaviors within the period.

Shown in Fig. 4 is the effect of contact time on the catalytic performance of 30 mol% $SrCl_2/CeO_2$, 30 mol%

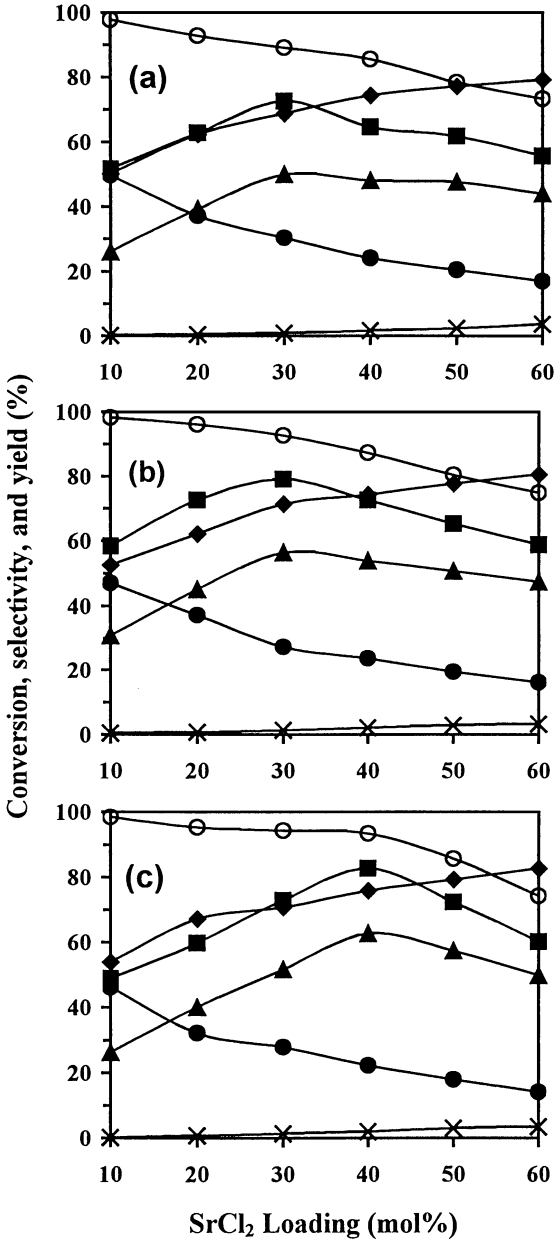

FIG. 2. Catalytic performance of (a) $SrCl_2/CeO_2$, (b) $SrCl_2/PrO_{1.83}$, and (c) $SrCl_2/TbO_{1.75}$ at 660°C and 1.67×10^{-4} h g mL^{-1} as related to $SrCl_2$ loading: (■) C_2H_6 conversion, (◆) C_2H_4 selectivity, (▲) C_2H_4 yield, (×) CH_4 selectivity, and (○) O_2 conversion.

TABLE 2

Catalytic Performance of REO_x, 30 mol% $SrCl_2/CeO_2$, 30 mol% $SrCl_2/PrO_{1.83}$, and 40 mol% $SrCl_2/TbO_{1.75}$ in the Oxidation of Ethane and Ethene at 660°C and 1.67×10^{-4} h g mL^{-1}

	Oxidation of C_2H_4[a]			Oxidation of C_2H_6		
Catalyst	C_2H_4 Conversion (%)	CO/CO_2 Ratio	Rate of C_2H_4 reaction 10^{18} molecules m^{-2} s^{-1}	C_2H_6 Conversion (%)	C_2H_4 Selectivity (%)	CO/CO_2 Ratio
CeO_2	27.6	1/26.7	0.134	31.6	30.2	0
$PrO_{1.83}$	31.2	1/30.8	0.144	35.4	24.6	0
$TbO_{1.75}$	21.5	1/20.6	0.138	41.2	36.4	0
$SrCl_2/CeO_2$	12.4	1/5.5	0.075	72.6	68.8	1/8.2
$SrCl_2/PrO_{1.83}$	14.7	1/6.8	0.083	79.1	71.4	1/7.5
$SrCl_2/TbO_{1.75}$	10.2	1/3.7	0.070	82.6	75.8	1/4.2

[a] At $C_2H_4/O_2/N_2$ molar ratio = 2/1/3.7.

$SrCl_2/PrO_{1.83}$, and 40 mol% $SrCl_2/TbO_{1.75}$ at 660°C. With the prolongation of contact time from 0.56×10^{-4} to 2.50×10^{-4} h g mL^{-1}, C_2H_6 conversion and CO_x selectivity increased, respectively, from 31.8 and 21.5% to 78.8 and 38.1% over the first catalyst, from 41.9 and 18.1% to 83.6 and 36.8% over the second catalyst, and from 36.7 and 16.2% to 85.4 and 30.7% over the third catalyst; the C_2H_4 selectivities decreased, respectively, from 78.3 to 60.3%, from 81.5 to 61.4%, and from 83.1 to 66.6%. The highest C_2H_4 yield was achieved at 1.25×10^{-4} h g mL^{-1} over 30 mol% $SrCl_2/PrO_{1.83}$ (57.2%), and at 1.67×10^{-4} h g mL^{-1} over 30 mol% $SrCl_2/CeO_2$ (49.9%) and 40 mol% $SrCl_2/TbO_{1.75}$ (62.6%). When the catalysts were dispersed in quartz sand (80–100 mesh, 5.0 g), we observed similar results.

XRD, BET, and Chlorine Composition Analysis Studies

Table 3 summarizes the crystal phases and surface areas of the undoped and $SrCl_2$-doped catalysts. After ODE reactions, the surface areas of the REO_x (RE = Ce, Pr, Tb), 30 mol% $SrCl_2/CeO_2$, 30 mol% $SrCl_2/PrO_{1.83}$, and 40 mol% $SrCl_2/TbO_{1.75}$ catalysts decreased by ca. 17, 12, 16, 17, 9, and 10%, respectively. No new phases were detected by XRD in the three undoped catalysts, but moderately intense signals of rhombohedral PrOCl and very weak signals of rhombohedral TbOCl were detected over the $SrCl_2$-doped praseodymium and terbium oxides, respectively. After 60 h of ODE reaction, very weak signals of orthorhombic $SrCO_3$ were observed over the three $SrCl_2$-promoted catalysts.

The surface and bulk chloride compositions of the 30 mol% $SrCl_2/REO_x$ catalysts are shown in Table 4. The Cl content on the surface is much higher than that in the bulk for the $SrCl_2$-doped CeO_2 catalyst, whereas the Cl concentration on the surface and that in the bulk are rather close for the other two catalysts. Compared to the original values, after 60 h of onstream ODE reaction, the concentrations of surface Cl decreased by 24.2, 11.4, and 2.1%, respectively; as for the bulk concentration, it decreased, respectively, by 33.3, 5.1, and 1.7%.

We used the least-squares refinement method to calculate the lattice parameters according to the d values of XRD patterns, with REO_x and $SrCl_2$ being supposed to fit a cubic and hexagonal symmetry, respectively. The results are summarized in Table 5. Compared to the lattice parameters in the PDF-2 files, the a value of the cubic REO_x lattice was enlarged by ca. 0.740% in 30 mol% $SrCl_2/CeO_2$, ca. 1.116% in 30 mol% $SrCl_2/PrO_{1.83}$, and ca. 1.639% in 40 mol% $SrCl_2/TbO_{1.75}$; however, the a and c values of the hexagonal $SrCl_2$ lattice were contracted by ca. 0.275 and 0.284% in 30 mol% $SrCl_2/CeO_2$, ca. 0.630 and 0.664% in 30 mol% $SrCl_2/PrO_{1.83}$, and ca. 1.150 and 1.166% in 40 mol% $SrCl_2/TbO_{1.75}$. Obviously, the $TbO_{1.75}$ lattice was the most significantly enlarged and the $SrCl_2$ lattice in 40 mol% $SrCl_2/TbO_{1.75}$ was the most pronouncedly contracted.

XPS Studies

Figure 5 shows the Ce 3d, Pr 3d, and Tb 4d spectra of the REO_x, 30 mol% $SrCl_2/CeO_2$, 30 mol% $SrCl_2/PrO_{1.83}$, and 40 mol% $SrCl_2/TbO_{1.75}$ samples treated under various conditions. From Fig. 5Ia, one can observe two sets of spin–orbit multiplets: u and v correspond to the $3d_{3/2}$ and $3d_{5/2}$ contributions, respectively; the Ce 3d spectrum contains three main $3d_{5/2}$ features at ca. 882.5 (v), 889.4 (v_2), and 898.7 eV (v_3) and three main $3d_{3/2}$ features at ca. 900.6 (u), 907.7 (u_2), and 916.6 eV (u_3); u_3 and v_3 could be assigned to the $3d^9\,4f^0$ photoemission final state, whereas either (v, v_2) or (u, u_2) doublets could be attributed to final states with strong mixing of the $3d^9\,4f^2$ and $3d^9\,4f^1$ configurations. These states arise from the core hole potential in the final state and 4f hybridization in the initial state (50–55). The shake-down v/v_2 and u/u_2 features occur due to the charge transfer from ligand (O 2p) to metal (Ce 4f), generating states of nominal metal charge +3 and +4. As for states v_1 at 885.6 eV and u_1 at 903.9 eV, according

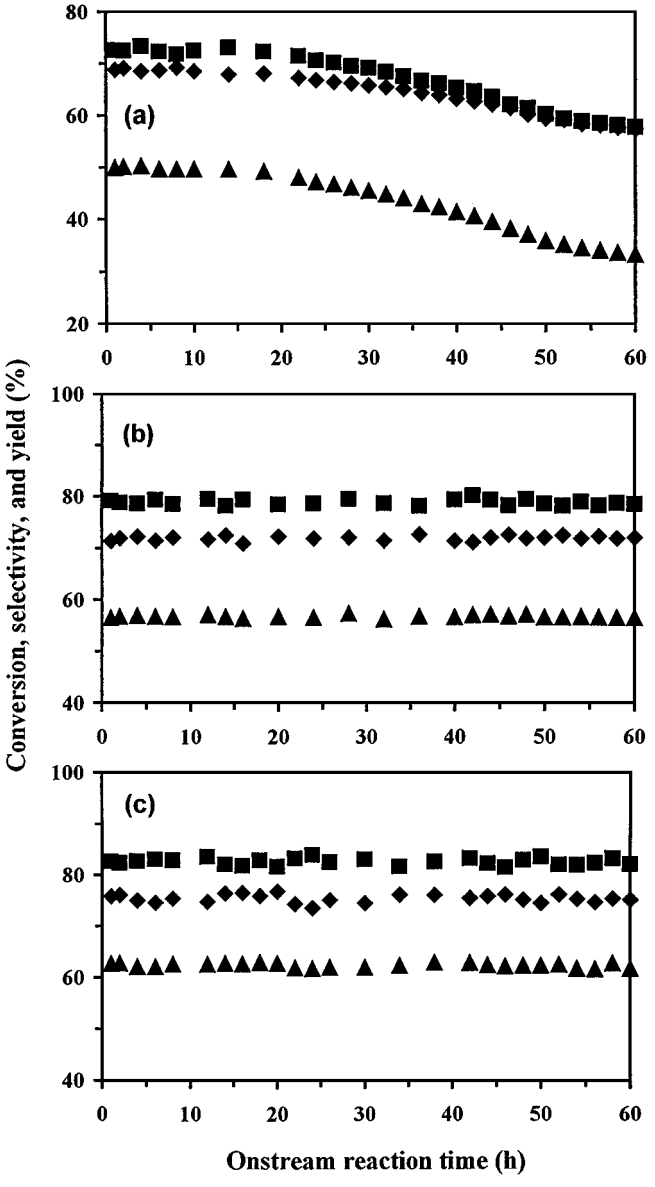

FIG. 3. Catalytic performance of (a) 30 mol% $SrCl_2/CeO_2$, (b) 30 mol% $SrCl_2/PrO_{1.83}$, and (c) 40 mol% $SrCl_2/TbO_{1.75}$ as related to onstream reaction time at 660°C and 1.67×10^{-4} h g ml^{-1} : (■) C_2H_6 conversion, (◆) C_2H_4 selectivity, and (▲) C_2H_4 yield.

to the assignment convention proposed by Burroughs *et al.* (56), they belong to unique photoelectron features from the Ce^{3+} state (which also exhibits features similar to the u_2 and v_2 features). On treating the Ce-containing samples in He at room temperature, one can see that 30 mol% $SrCl_2/CeO_2$ (Fig. 5Ia′) contained more Ce^{3+} ions than CeO_2 (Fig. 5Ia). With the rise in H_2 treatment temperature from 510 to 600, and then to 900°C, the v_1 and u_1 components increased in intensity and the intensities of the signals due to Ce^{3+} in the $SrCl_2$-doped CeO_2 samples (Figs. 5Ib′–5Id′) increased much more obviously than those in the undoped CeO_2 samples (Figs. 5Ib–5Id). In the Pr 3*d* profiles of $PrO_{1.83}$ and 30 mol% $SrCl_2/PrO_{1.83}$, two sets of spin–orbit multiples are observed at binding energies of ca. 953.5 and 933.9 eV, representing $3d_{3/2}$ and $3d_{5/2}$, respectively. According to Matsumura *et al.* (57) and Sarma and Rao (58), we assign the signals at ca. 933.9, 953.5, and 966.9 eV to Pr^{4+} and the signals at ca. 929.5, 949.8, and 973.2 eV to Pr^{3+}. From the relative intensity of the signals due to Pr^{4+} and those due to Pr^{3+} (Figs. 5IIa and 5IIa′), one can see that there are more Pr^{3+} ions in the $SrCl_2$-doped sample than in the undoped one. The rise in H_2 reduction temperature caused the signals of Pr^{3+} to increase in intensity for the undoped and $SrCl_2$-doped $PrO_{1.83}$ samples (Figs. 5IIb–5IId and 5IIb′–5IId′). By comparing the Tb 4*d* spectrum of $TbO_{1.75}$ (Fig. 5IIIa) with those

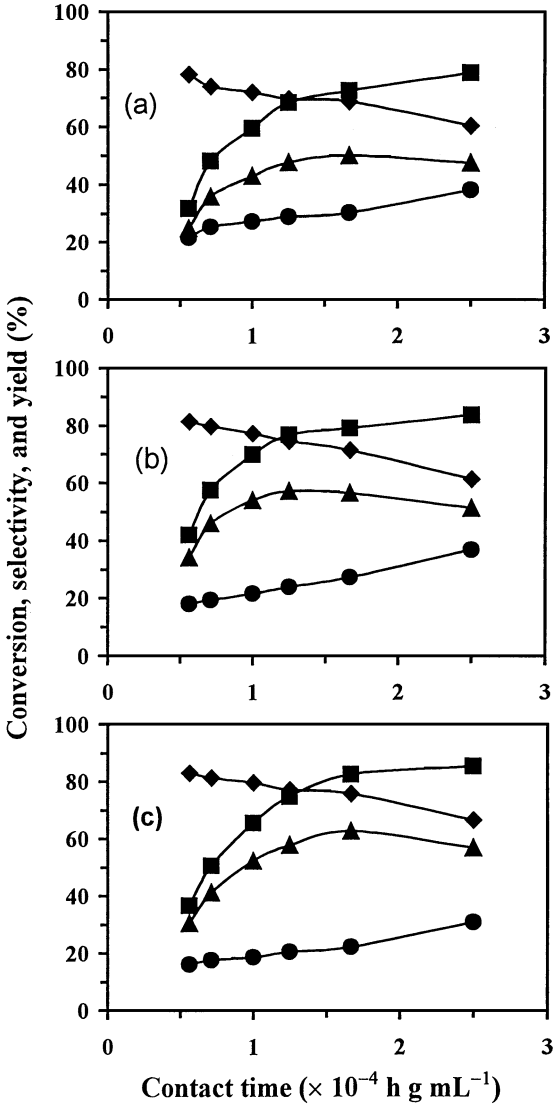

FIG. 4. Catalytic performance of (a) 30 mol% $SrCl_2/CeO_2$, (b) 30 mol% $SrCl_2/PrO_{1.83}$, and (c) 40 mol% $SrCl_2/TbO_{1.75}$ at 660°C as a function of contact time: (■) C_2H_6 conversion, (◆) C_2H_4 selectivity, (▲) C_2H_4 yield, and (●) CO_x selectivity.

TABLE 3

Crystal Phase and Surface Areas of REO_x, 30 mol% $SrCl_2/CeO_2$, 30 mol% $SrCl_2/PrO_{1.83}$, and 40 mol% $SrCl_2/TbO_{1.75}$ Catalysts Measured before and after ODE Reaction at 660°C for 60 h

Catalyst	Crystal phase[a]		Surface area ($m^2\,g^{-1}$)	
	Before	After	Before	After
CeO_2	CeO_2 (s)	CeO_2 (s)	4.1	3.4[b]
$PrO_{1.83}$	$PrO_{1.83}$ (s)	$PrO_{1.83}$ (s)	4.3	3.8[b]
$TbO_{1.75}$	$TbO_{1.75}$ (s)	$TbO_{1.75}$ (s)	3.1	2.6[b]
$SrCl_2/CeO_2$	CeO_2 (s), $SrCl_2 \cdot 6H_2O$ (m)	CeO_2 (s), $SrCO_3$ (vw), $SrCl_2 \cdot 6H_2O$ (m)	3.3	2.8
$SrCl_2/PrO_{1.83}$	$PrO_{1.83}$ (s), PrOCl (m) $SrCl_2 \cdot 6H_2O$ (m)	$PrO_{1.83}$ (s), PrOCl (m), $SrCO_3$ (vw), $SrCl_2 \cdot 6H_2O$ (m)	3.5	3.2
$SrCl_2/TbO_{1.75}$	$TbO_{1.75}$ (s), TbOCl (vw), $SrCl_2 \cdot 6H_2O$ (m)	$TbO_{1.75}$ (s), TbOCl (vw), $SrCO_3$ (vw), $SrCl_2 \cdot 6H_2O$ (m)	2.9	2.6

[a] CeO_2, $PrO_{1.83}$, and $TbO_{1.75}$ are cubic. PrOCl and TbOCl are rhombohedral. $SrCO_3$ is orthorhombic. $SrCl_2 \cdot 6H_2O$ is hexagonal. s, strong; m, medium; vw, very weak.

[b] 8 h of onstream ODE reation.

of $TbO_{1.50}$ and TbO_2 (59), one can assign the signals at ca. 156.9 and 164.5 eV to the characteristic features of Tb^{4+} and the signal at ca. 149.3 eV to Tb^{3+} (58, 59). Apparently, Tb^{4+} and Tb^{3+} are present in the $TbO_{1.75}$ sample and the concentration of Tb^{3+} ions in the $SrCl_2$-doped sample (Fig. 5IIIa′) was larger than that in the undoped one (Fig. 5IIIa). With the increase in reduction temperature (Figs. 5IIIb–5IIId), the intensities of the signals due to Tb^{4+} declined, whereas those due to Tb^{3+} increased. For the 40 mol% $SrCl_2/TbO_{1.75}$ sample, the intensities of the signals at ca. 156.9 and 164.5 eV were lower whereas the intensity of the signals at ca. 149.3 eV was higher than those in the $TbO_{1.75}$ sample, indicating that there are more Tb^{3+} in the $SrCl_2$-doped catalyst than in the undoped one. With increasing H_2 treatment temperature (Figs. 5IIIb′–5IIId′), the signals due to Tb^{3+} increased while the signals due to Tb^{4+} decreased in intensity.

Shown in Fig. 6 are the O 1*s* spectra of the REO_x, 30 mol% $SrCl_2/CeO_2$, 30 mol% $SrCl_2/PrO_{1.83}$, and 40 mol% $SrCl_2/TbO_{1.75}$ samples treated under various conditions. After treatment in He at room temperature, there are two O 1*s* peaks at ca. 529.5 and 531.5 eV for all the samples (Figs. 6Ia–6IIIa and 6Ia′–6IIIa′). We assign the signal at lower binding energy (529.5 eV) to surface lattice oxygen and the signal at higher binding energy (531.5 eV) to adsorbed oxygen species such as O^-, O_2^{2-}, or O_2^- (60–63). The O 1*s* binding energy of OH^- also falls in the 531–532 eV range. In order to eliminate the possibility of OH^- presence, we had heated the samples in an O_2 flow at 800°C for 1 h before the XPS measurement. One can observe that with the rise in H_2 treatment temperature from 500 to 800 or 900°C, the component at ca. 531.5 eV decreased in intensity and disappeared at or above 800°C, whereas the intensity of the component at ca. 529.5 eV increased (Figs. 6I–6III).

TABLE 4

Surface and Bulk Chloride Compositions of 30 mol% $SrCl_2/CeO_2$, 30 mol% $SrCl_2/PrO_{1.83}$, and 40 mol% $SrCl_2/TbO_{1.75}$ Catalysts Estimated According to the Results of XPS and Chemical Analyses, Respectively

Catalyst	Surface composition (wt%)		Bulk composition (wt%)	
	Before	After[a]	Before	After[a]
$SrCl_2/CeO_2$	18.77	14.23	12.54	8.36
$SrCl_2/PrO_{1.83}$	2.98	2.64	2.73	2.59
$SrCl_2/TbO_{1.75}$	5.69	5.57	5.46	5.37

[a] After 60 h of ODE reaction at 660°C.

TABLE 5

Lattice Parameters of REO_x and $SrCl_2$ Phases in the 30 mol% $SrCl_2/CeO_2$, 30 mol% $SrCl_2/PrO_{1.83}$, and 40 mol% $SrCl_2/TbO_{1.75}$ Catalysts Calculated According to the *d* Values of XRD Patterns

Catalyst	Crystal phase	Lattice parameter (Å)		
		a	*b*	*c*
$SrCl_2/CeO_2$	CeO_2	5.4514 (5.41134)	5.4514 (5.41134)	5.4514 (5.41134)
	$SrCl_2$	7.9411 (7.9630)	7.9411 (7.9630)	4.1133 (4.1250)
$SrCl_2/PrO_{1.83}$	$PrO_{1.83}$	5.5288 (5.4678)	5.5288 (5.4678)	5.5288 (5.4678)
	$SrCl_2$	7.9128	7.9128	4.0976
$SrCl_2/TbO_{1.75}$	$TbO_{1.75}$	5.4021 (5.315)	5.4021 (5.315)	5.4021 (5.315)
	$SrCl_2$	7.8714	7.8714	4.0769

Note: The values in parentheses are the PDF-2 data of the pure compounds.

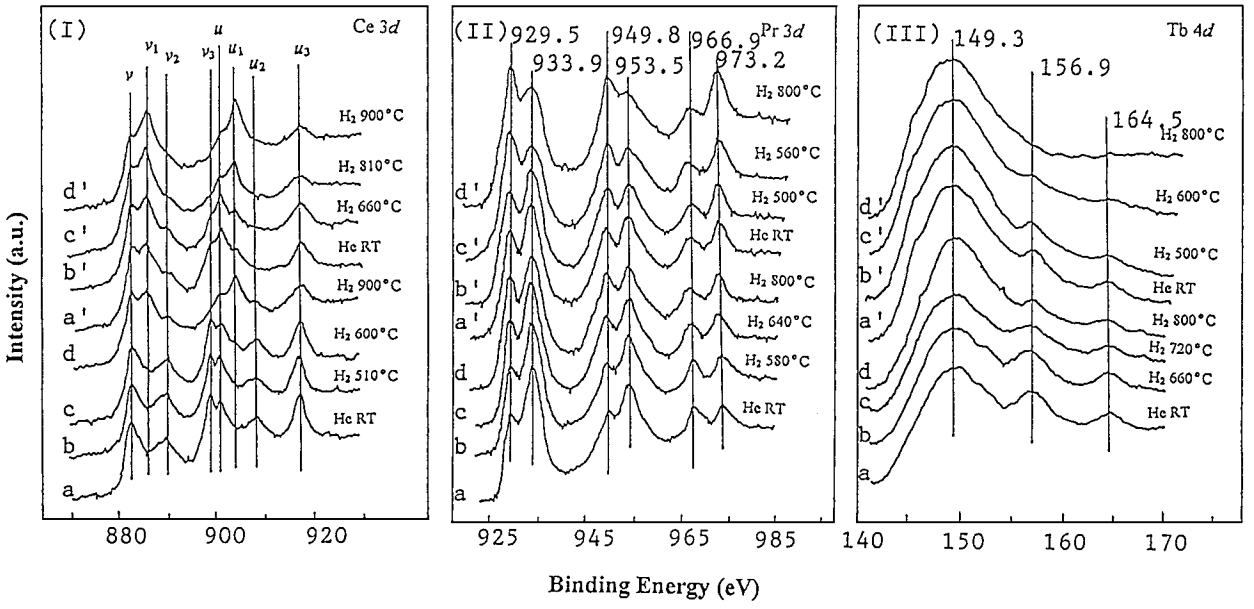

FIG. 5. Ce 3*d*, Pr 3*d*, and Tb 4*d* XPS spectra of the (I) CeO_2 (a–d) and 30 mol% $SrCl_2/CeO_2$ (a′–d′), (II) $PrO_{1.83}$ (a–d) and 30 mol% $SrCl_2/PrO_{1.83}$ (a′–d′), and (III) $TbO_{1.75}$ (a–d) and 40 mol% $SrCl_2/TbO_{1.75}$ (a′–d′) samples treated under various conditions. RT denotes room temperature.

$^{18}O_2$- and C_2H_6-Pulsing Studies

To confirm the involvement of lattice oxygen in the ODE reaction, we performed $^{18}O_2$- and C_2H_6-pulsing experiments on the 30 mol% $SrCl_2/CeO_2$, 30 mol% $SrCl_2/PrO_{1.83}$, and 40 mol% $SrCl_2/TbO_{1.75}$ samples which had been treated in He (20 mL min^{-1}) at 840, 560, and 600°C, respectively, for 15 min. After pulsing C_2H_6 at 660°C onto the $^{18}O_2$-treated catalysts, besides the signals due to C_2H_6 and C_2H_4, we detected signals at $m/e = 20$, 19, and 18, corresponding to $H_2{}^{18}O$, ^{18}OH, and ^{18}O, respectively; the intensities of the three ^{18}O-containing species for $SrCl_2$-doped CeO_2 were

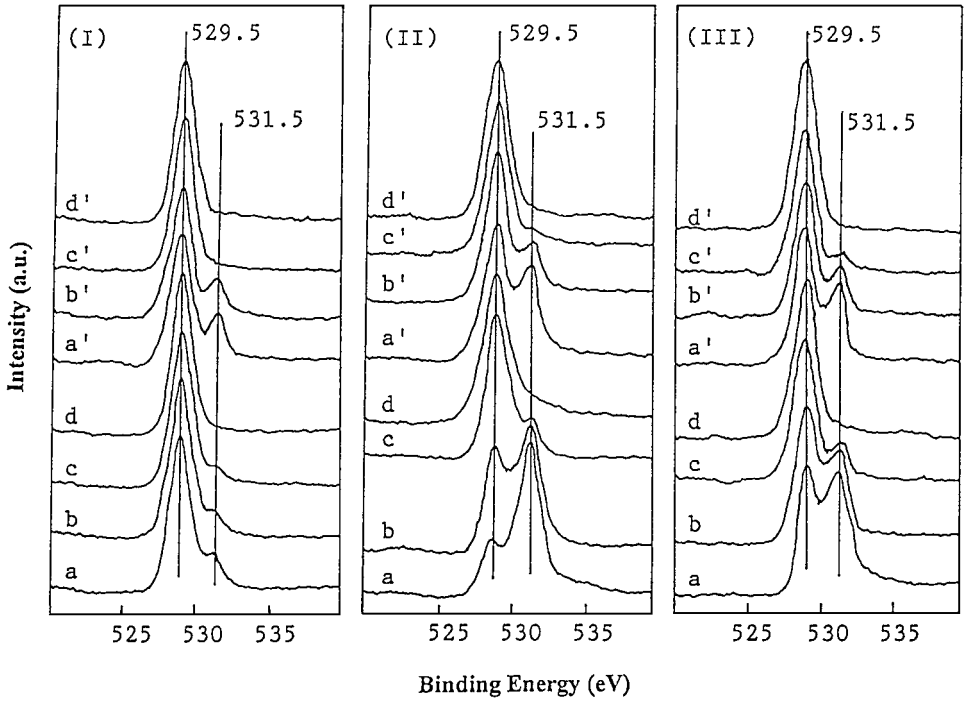

FIG. 6. O 1*s* XPS spectra of the (I) CeO_2 (a–d) and 30 mol% $SrCl_2/CeO_2$ (a′–d′), (II) $PrO_{1.83}$ (a–d) and 30 mol% $SrCl_2/PrO_{1.83}$ (a′–d′), and (III) $TbO_{1.75}$ (a–d) and 40 mol% $SrCl_2/TbO_{1.75}$ (a′–d′) samples treated under various conditions. (a–d) and (a′–d′) are the same as those in Fig. 5.

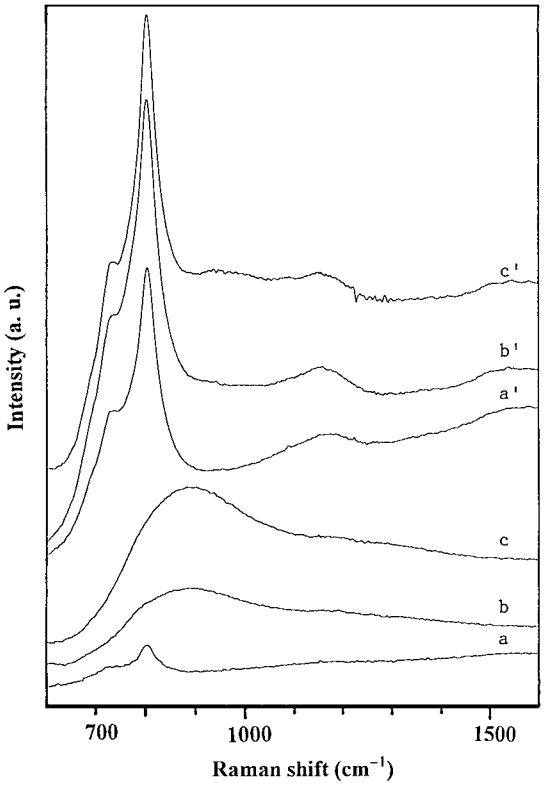

FIG. 7. *In situ* Raman spectra of CeO_2 (a–c) and 30 mol% $SrCl_2/CeO_2$ (a′–c′) when the catalysts were treated (a, a′) in O_2 at 800°C for 15 min, (b, b′) then in H_2 at 900°C for 15 min and in O_2 at 660°C for 5 min, and (c, c′) then in H_2 at 900°C for 15 min and in $C_2H_6/O_2/N_2$ (molar ratio, 2/1/3.7) at 660°C for 5 min.

much lower than those for $SrCl_2$-doped $PrO_{1.83}$ or $TbO_{1.75}$. These results indicate that lattice $^{18}O^{2-}$ (incorporated in the REO_x lattice via $^{18}O/^{16}O$ exchange during $^{18}O_2$-pulsing) had reacted with C_2H_6 and the activity of lattice oxygen at 660°C in 30 mol% $SrCl_2/CeO_2$ was much lower than that of 30 mol% $SrCl_2/PrO_{1.83}$ or 40 mol% $SrCl_2/TbO_{1.75}$.

In Situ Raman Spectroscopic Studies

Since $PrO_{1.83}$ and $TbO_{1.75}$ as well as their $SrCl_2$-doped counterparts are black and dark brown in color, respectively, they are Raman-silent. Figure 7 illustrates the *in situ* Raman spectra of CeO_2 and 30 mol% $SrCl_2/CeO_2$ which are light yellow in color under various treatment conditions. When both samples were treated in O_2 (20 mL min^{-1}) at 800°C for 15 min, a very weak Raman band at ca. 803 cm^{-1} over CeO_2 (Fig. 7a) and three bands at ca. 727, 802, and 1163 cm^{-1} over 30 mol% $SrCl_2/CeO_2$ (Fig. 7a′) were observed. Since the Raman bands attributable to lattice vibrations of undoped and halide-doped CeO_2 appeared only below 500 cm^{-1} (47, 49, 64), we assign the signals within the range of 720–900 cm^{-1} to O_2^{2-} and the signal at 1163 cm^{-1} to O_2^- (25, 47, 49, 65–67). On exposing the samples which had just been treated in H_2 (20 mL min^{-1}, at 800°C for 10 min) to an O_2 flow at 660°C for 10 min, the Raman band of the CeO_2 sample shifted to ca. 880 cm^{-1} and increased in intensity (Fig. 7b); for the $SrCl_2$-doped sample, the intensity of the signals at ca. 727 and 802 cm^{-1} increased significantly in intensity (Fig. 7b′). After treatment of the CeO_2 and 30 mol% $SrCl_2/CeO_2$ catalysts (which had just been reduced by H_2 at 900°C for 10 min, respectively) in a reactant flow ($C_2H_6/O_2/N_2$ molar ratio = 2/1/3.7, 20 mL min^{-1}) at 660°C for 10 min, the spectrum shape and the signal positions (Fig. 7c′) were similar to those obtained after O_2 treatment at the same temperature (Fig. 7b′) for the $SrCl_2$-doped sample, but the intensity of the signal at 880 cm^{-1} increased markedly for the undoped CeO_2 sample (Fig. 7c).

O_2-TPD and TPR Studies

Figure 8 illustrates the O_2-TPD profiles of the REO_x, 30 mol% $SrCl_2/CeO_2$, 30 mol% $SrCl_2/PrO_{1.83}$, and 40 mol% $SrCl_2/TbO_{1.75}$ samples. For CeO_2, there were two peaks at ca. 716 and 810°C (Fig. 8a); the total amount of O_2 desorption was 1.88 μmol g^{-1}. For $PrO_{1.83}$, there were four desorptions at ca. 252, 313, 369, and 459°C (a total of 365.42 μmol g^{-1}) and two desorptions at ca. 737 and 871°C

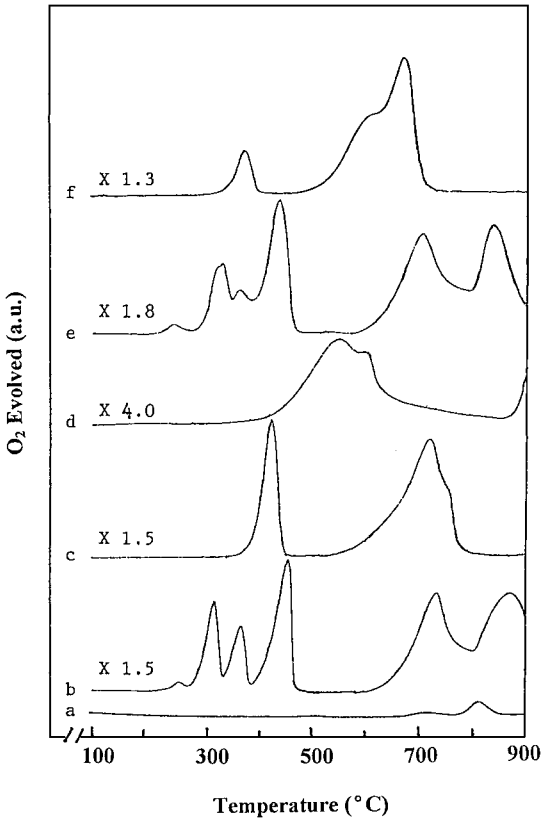

FIG. 8. O_2-TPD profiles of (a) CeO_2, (b) $PrO_{1.83}$, (c) $TbO_{1.75}$, (d) 30 mol% $SrCl_2/CeO_2$, (e) 30 mol% $SrCl_2/PrO_{1.83}$, and (f) 40 mol% $SrCl_2/TbO_{1.75}$ catalysts.

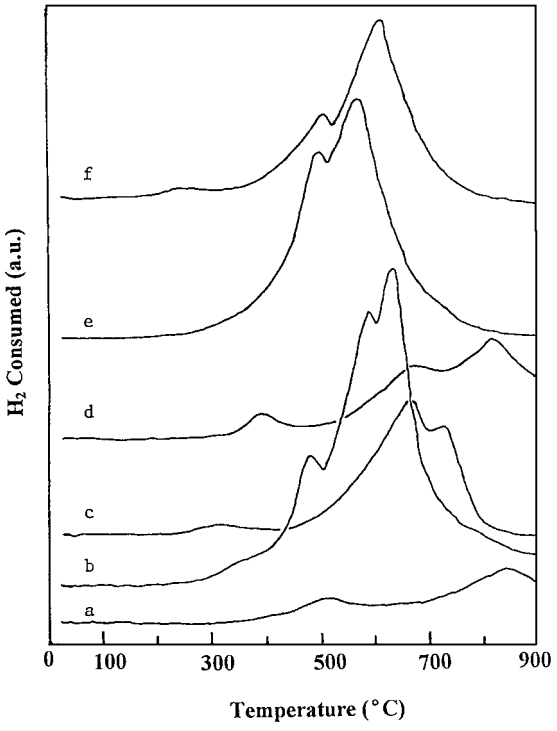

FIG. 9. TPR profiles of (a) CeO_2, (b) $PrO_{1.83}$, (c) $TbO_{1.75}$, (d) 30 mol% $SrCl_2/CeO_2$, (e) 30 mol% $SrCl_2/PrO_{1.83}$, and (f) 40 mol% $SrCl_2/TbO_{1.75}$ catalysts.

(a total of 338.92 μmol g^{-1}) (Fig. 8b). As for $TbO_{1.75}$, three desorption peaks appeared at ca. 427 (314.64 μmol g^{-1}), 722, and 755°C (a total of 474.60 μmol g^{-1}) (Fig. 8c). Over the $SrCl_2$-doped CeO_2 sample, two peaks at ca. 550 and 600°C (a total of 37.71 μmol g^{-1}) and a large one starting at ca. 860°C were observed (Fig. 8d). For the $SrCl_2$-doped $PrO_{1.83}$ sample, six peaks appeared at ca. 236, 325, 364, 440, 705, and 839°C, with the first four peaks amounting totally to 213.53 μmol g^{-1} of O_2 desorption and the last two peaks to 623.03 μmol g^{-1} of O_2 desorption (Fig. 8e). Only three signals at ca. 375, 615, and 679°C were recorded for the $SrCl_2$-doped $TbO_{1.75}$ sample (Fig. 8f), with the first peak corresponding to 63.62 μmol g^{-1} and the other two peaks to 510.32 μmol g^{-1} of O_2 desorption.

Figure 9 shows the TPR profiles of the REO_x, 30 mol% $SrCl_2/CeO_2$, 30 mol% $SrCl_2/PrO_{1.83}$, and 40 mol% $SrCl_2/TbO_{1.75}$ samples. We observed two reduction bands at ca. 508 and 844°C for CeO_2 (Fig. 9a), four reduction bands at ca. 350, 469, 580, and 640°C for $PrO_{1.83}$ (Fig. 9b), and three reduction bands at ca. 303, 667, and 720°C for $TbO_{1.75}$ (Fig. 9c); the band(s) at lower temperature is/are much smaller than that at higher temperature. Three bands are observed at ca. 389, 664, and 814°C for 30 mol% $SrCl_2/CeO_2$ (Fig. 9d) and two bands at ca. 493 and 559°C for 30 mol% $SrCl_2/PrO_{1.83}$ (Fig. 9e), and three bands at ca. 250, 495, and 599°C for 40 mol% $SrCl_2/TbO_{1.75}$ (Fig. 9f). One can also see that the addition of $SrCl_2$ to REO_x caused the reduction bands to shift to lower temperatures. We also observed that after the O_2-TPD and TPR experiments, the color of CeO_2 (with the exception in O_2-TPD) and 30 mol% $SrCl_2/CeO_2$ changed from white-yellow to light yellow-green, that of $PrO_{1.83}$ and 30 mol% $SrCl_2/PrO_{1.83}$ from black to light yellow-green, and that of $TbO_{1.75}$ and 40 mol% $SrCl_2/TbO_{1.75}$ from dark brown to white.

DISCUSSION

Improvement in Catalytic Performance by $SrCl_2$ Doping

A large number of rare earth oxides have been tested as OCM or ODE catalysts (e.g., 17, 18, 44, 46–49, 68–73). Most of them showed moderate catalytic activity. Adding promoters such as alkali metal oxides (20), MO (M = alkaline earth metals) (20, 22, 25, 34, 74), and MX_2 (X = F, Cl, Br) (22, 25, 27, 30, 47, 74) to the lanthanide oxides could improve their catalytic abilities. For the ODE reaction, as shown in Table 1 and Fig. 1, the single-component REO_x (RE = Ce, Pr, Tb) catalysts performed moderately well; with the doping of $SrCl_2$ into the three oxides, the C_2H_6 conversion and C_2H_4 selectivity was enhanced significantly. From Fig. 2, one can observe that, at a 30 mol% loading of $SrCl_2$ (40 mol% for $TbO_{1.75}$) in the $SrCl_2$-promoted REO_x catalysts, the C_2H_4 yield was at its maximum. During the 60 h of onstream reaction, the 30 mol% $SrCl_2/CeO_2$ catalyst deactivated (Fig. 3a), whereas the 30 mol% $SrCl_2/PrO_{1.83}$ and 40 mol% $SrCl_2/TbO_{1.75}$ catalysts showed stable activities (Figs. 3b and 3c). In the contact time studies (Fig. 4), with the prolongation of contact time, the C_2H_6 conversion and CO_x selectivity increased, while the C_2H_4 selectivity decreased. Similar results were observed when the three $SrCl_2$-modified REO_x catalysts were well dispersed in quartz sand, implying that the obvious enhancement in catalytic performance is a result of catalytic action rather than a result of hot spot generation. Besides the improved catalytic behaviors, the introduction of $SrCl_2$ to REO_x caused the O_2 conversions at high C_2H_6 conversions and high C_2H_4 selectivities to drop (Table 1). This is understandable because an enhancement in C_2H_4 selectivity signals the dominance of the ODE reaction, in which a smaller amount of O_2 can convert a relatively larger amount of C_2H_6 as compared to the deep oxidation reactions. It should be noted that when the reaction temperature was at or above 660°C, the C_2H_4 selectivity decreased, whereas CH_4 and CO_x selectivities increased over the $SrCl_2$-doped catalysts. Methane generation was suggested to follow two possible routes: (i) ethane decomposition in the gas phase and (ii) a heterogeneous pathway involving an ethylperoxy intermediate (18). Ethylperoxy reacted with surface oxygen species to form CH_4 and HCO_2; the latter was further oxidized to CO_x. Compared to the results of ODE reaction above 600°C over the 30 mol% BaX_2/Y_2O_3 (X = F, Cl, Br) (25) and 40 mol% $SrCl_2/Ln_2O_3$ (Ln = Sm, Nd) (26) catalysts,

the amounts of CH_4 formed over the $SrCl_2$-promoted REO_x ($RE = $ Ce, Pr, Tb) catalysts under similar conditions were much smaller. The activation of CO_2 has been reported by Trovarelli *et al.* (75–77) to be strongly enhanced in the presence of Ce^{3+} sites. Materials such as PrO_x (78), TbO_x (78), and CaO–CeO_2 (79) have also been reported as effective catalysts for CH_4 conversion in the presence of CO_2. Similar behaviors could be expected for the $SrCl_2$-modified REO_x catalysts. We suggest that over the reducible oxide catalysts the interaction of CH_4 and CO_2 formed during the ODE reaction would produce C_2H_4 and CO. Considering C_2H_4 selectivities and C_2H_6 conversions of the catalysts under similar reaction conditions (for example, at 660°C and at ca. 90% O_2 conversion), we conclude that the catalytic performance of REO_x and $SrCl_2$-promoted REO_x increased in the order $PrO_{1.83} \approx CeO_2 < TbO_{1.75} <$ 30 mol% $SrCl_2/CeO_2 <$ 30 mol% $SrCl_2/PrO_{1.83} <$ 40 mol% $SrCl_2/TbO_{1.75}$.

In the $SrCl_2/REO_x$ catalysts, chloride ions have a positive effect on the catalytic performance. The presence of Cl^- ions on the chloride-promoted oxide catalyst surfaces could eliminate the sites for complete oxidation and could create new active sites for the selective oxidation of C_2H_6 to C_2H_4 (80). Shi *et al.* (81) evidenced experimentally that C_2H_4 was the predominant source for CO_x formation at or above 650°C. In other words, if the deep oxidation of C_2H_4 could be reduced or avoided, C_2H_4 selectivity would be augmented. Compared to the REO_x catalysts, the chloride-modified counterparts exhibited much lower C_2H_4 conversions in the C_2H_4 oxidation reaction and much higher C_2H_4 selectivities in the ODE reaction (Table 2), indicating that $SrCl_2$ doping reduced C_2H_4 deep oxidation markedly. Furthermore, the noticeable increase of CO/CO_2 ratios in the reaction products over the $SrCl_2$-doped REO_x catalysts is an indication of the reduction in C_{2+} deep oxidation reactions. Similar effects were observed over the BaX_2-doped Y_2O_3 (25) and Ho_2O_3 (74) catalysts. Therefore, we conclude that the addition of $SrCl_2$ can reduce the deep oxidation of C_2H_4 formed in the ODE reaction and thus enhance significantly the C_2H_4 selectivity.

Defect Structure Induced by $SrCl_2$ Modification

As shown in the XRD results (Table 3), for the fresh $SrCl_2$-doped catalysts, phases of rhombohedral PrOCl (medium signal intensity) and TbOCl (very weak signal intensity) were detected but that of CeOCl was not. By introducing CCl_4 to the ODE feedstream at 700°C, Sugiyama *et al.* (17) observed the formation of CeOCl. After studying the destructive adsorption of CCl_4 at ca. 450°C on CeO_2 by XPS and *in situ* Raman spectroscopy, Weckhuysen *et al.* (64) observed the reduction of Ce^{4+} to Ce^{3+} and the formation of CeOCl. In another paper, however, Sugiyama *et al.* (82) reported the absence of CeOCl phase when CeO_2 was exposed to a feedstream containing CCl_4 at 750°C. Indeed, on the basis of the heat of formation for $REOCl$ from the corresponding oxide (82–84), one can deduce that the formation of CeOCl is the most difficult among the three oxychlorides. The existence of PrOF and TbOF with different XRD signal intensities and the nonexistence of CeOF were also reported in the study of BaF_2-modified $PrO_{1.83}$, $TbO_{1.75}$, and CeO_2 catalysts (46). One can realize from Table 3 that the crystal structures of REO_x in the undoped catalysts remained unaltered after 8 or 60 h of onstream reaction. As for the $SrCl_2$-doped ones, we detected weak signals of orthorhombic $SrCO_3$ phase after 60 h. The surface areas of the undoped catalysts reduced by 12–17%, whereas those of the $SrCl_2$-promoted $PrO_{1.83}$ and $TbO_{1.75}$ decreased by less than 10% (the 30 mol% $SrCl_2/CeO_2$ catalyst reduced by 17% in surface area) after 60 h of ODE reaction. This indicates that the stabilization of surface areas is an essential factor for stable catalytic performance. From Table 4, it can be seen that the Cl compositions on the surface and in the bulk of the $SrCl_2$-modified $PrO_{1.83}$ and $TbO_{1.75}$ catalysts were rather similar, indicating a uniform distribution of Cl^- ions in the catalysts; but for the $SrCl_2$-modified CeO_2 catalyst, Cl^- segregation took place on the surface; this phenomenon might be responsible for the significant loss of chlorine during ODE reactions. Furthermore, the small difference in Cl^- concentration in the $SrCl_2$-doped $PrO_{1.83}$ or $TbO_{1.75}$ catalyst before and after 60 h of reaction means that Cl leaching was modest. The sustainable catalytic performance of 30 mol% $SrCl_2/PrO_{1.83}$ and 40 mol% $SrCl_2/TbO_{1.75}$ in 60 h of onstream reaction is supporting evidence for this deduction.

It has been generally accepted that ionic exchanges or substitutions take place between rare earth oxides and alkaline earth oxides or halides. The infiltration of Ca^{2+} (31) or Sr^{2+} (33) into the Y_2O_3 lattice led to the formation of defective structure. Filkova *et al.* (34) ascribed the better catalytic performance of the SrO-doped Nd_2O_3 catalyst to the incorporation of Sr into the Nd_2O_3 lattice. Previously, we proposed that the presence of SrF_2 in SmOF (22) and BaX_2 ($X =$ F, Cl, Br) in Y_2O_3 (25) or Nd_2O_3 (30) caused the rare earth oxyfluoride or oxide lattices to enlarge and the halide lattice to shrink due to partial ionic exchanges between the two phases. It should be pointed out that the partial conversion of RE^{4+} to RE^{3+}ions would also contribute to lattice expansion as suggested by Bauer and Gingerich (85), Ray *et al.* (86), and Perrichon *et al.* (87). The radius of Sr^{2+} ion (1.18 Å) is larger than that of Ce^{3+} (1.01 Å), Ce^{4+} (0.87 Å), Pr^{3+} (0.99 Å), Pr^{4+} (0.85 Å), Tb^{3+} (0.92 Å), or Tb^{4+} (0.76 Å), whereas an O^{2-} ion (radius, 1.40 Å) is smaller than a Cl^- ion (radius, 1.81 Å) (88). The ionic exchanges between $SrCl_2$ and REO_x would result in the enlargement of the REO_x lattice and the contraction of the $SrCl_2$ lattice in the $SrCl_2$-modified REO_x catalysts. In addition to the difference in ionic radius, lattice distortion is also strongly associated with the temperature adopted for catalyst calcination

(25, 89). Hence, we chose 900°C (which is near the melting point of $SrCl_2$) to calcine the catalysts for the maximal structural defects formation. The extent of ionic exchanges would determine the defect density and hence the catalytic activity. The addition of $SrCl_2$ modified the surface and bulk natures of REO_x as well as those of $SrCl_2$ itself. As shown in Table 5, the lattices of REO_x in the $SrCl_2$-doped catalysts were enlarged, whereas those of $SrCl_2$ in the three catalysts contracted. The extent of REO_x lattice expansion increased in the order of 30 mol% $SrCl_2/CeO_2$ < 30 mol% $SrCl_2/PrO_{1.83}$ < 40 mol% $SrCl_2/TbO_{1.75}$, indicating that the extent of $SrCl_2$ infiltration into the REO_x lattices increased according to the above sequence. In contrast, the extent of $SrCl_2$ lattice shrinking increased in the order of 30 mol% $SrCl_2/CeO_2$ < 30 mol% $SrCl_2/PrO_{1.83}$ < 40 mol% $SrCl_2/TbO_{1.75}$, implying that the degree of REO_x diffusion into the $SrCl_2$ lattice increased in the above order. Working on the Ba- and Cl-doped $Sm_2Sn_2O_7$ pyrochlore catalysts for OCM reactions, Roger *et al.* (90) pointed out that the O–Ba–Cl species formed in the process of catalyst preparation are responsible for the good catalytic performance of the doped catalysts. Similarly, due to the existence of ionic exchanges or substitutions between the $SrCl_2$ and REO_x phases, it is reasonable to consider the formation of the O–Sr–Cl, Cl–Sr–*RE*–Cl, O–Sr–*RE*–Cl or O–*RE*–Cl species in the $SrCl_2$-doped REO_x catalysts. The difference in C_2H_6 conversion and C_2H_4 selectivity might be associated with the distortions of the $SrCl_2$ and REO_x lattices. Therefore, it is understandable that the catalytic performance follows the sequence 40 mol% $SrCl_2/TbO_{1.75}$ (which contained the highest amounts of $SrCl_2$ in $TbO_{1.75}$ and of $TbO_{1.75}$ in $SrCl_2$) > 30 mol% $SrCl_2/PrO_{1.83}$ > 30 mol% $SrCl_2/CeO_2$ (which contained the lowest amounts of $SrCl_2$ in CeO_2 and of CeO_2 in $SrCl_2$). One, however, cannot deny the possible role(s) of PrOCl and/or TbOCl phase in the enhancement of catalytic performance.

Enhancement in RE Ion Redox Ability

After investigating $PrO_{1.83}$ and $TbO_{1.75}$ for the OCM reaction, Gaffney *et al.* (35) attributed the higher reactivity of the nonstoichiometric oxides to three factors: (i) rapid interconversion of oxidation states ($RE^{3+} \Leftrightarrow RE^{4+}$), (ii) rapid diffusion of O_2 in the bulk, and (iii) high RE^{4+}/RE^{3+} oxidation potentials. They also pointed out that the formation of defective $PrO_{1.83-\delta}$ structure, a result of the migration of a substantial amount of sodium into the lanthanide oxide lattice, promotes the redox behavior of Pr^{4+}/Pr^{3+} and thus enhances the regeneration of active species. Among the higher oxides of Ce, Pr, and Tb, the most oxidized form (mainly +4 oxidation state) in each case is the fluorite dioxide: CeO_2, PrO_2, and TbO_2. Each Pr_6O_{11} ($PrO_{1.83}$) and Tb_4O_7 ($TbO_{1.75}$) molecule could be considered to be composed of $4PrO_2 + Pr_2O_3$ ($PrO_{1.50}$) and $2TbO_2 + Tb_2O_3$ ($TbO_{1.50}$), respectively. $PrO_{1.83}$ and $TbO_{1.75}$ are oxygen-deficient fluorite-related structures because $PrO_{1.50-\delta}$ and $TbO_{1.50-\delta}$ contain one-fourth intrinsic oxygen vacancy (91). After reduction in a H_2 flow, respectively, at 900, 550, and 650°C (92), the three dioxides could be converted to $CeO_{1.50}$, $PrO_{1.50}$, and $TbO_{1.50}$ (mainly +3 oxidation state). In contrast, they are easily oxidized to the thermodynamically stable REO_2 form at lower temperatures, even at room temperature. For hydrocarbon oxidation reactions, the stabilization of RE^{3+} moieties in the catalyst would result in an enhanced activity of the catalyst because a number of oxygen vacancies have become available due to RE^{3+} formation. Therefore, a suitable RE^{4+}/RE^{3+} ratio is required for the three reducible rare earth oxides to be effective oxidation catalysts. It can be achieved by incorporating some aliovalent metal ions (Sr^{2+}) into the lattice of the parent oxide (REO_x). DeBoy and Hicks (93) interpreted the higher CH_4 conversion and the lower C_{2+} selectivity over PrO_x as due to the presence of Pr^{4+} species. Poirier *et al.* (36) believed that doping Li to PrO_x suppressed the formation of Pr^{4+} ions; this would be associated with the mobile oxygen responsible for the surface oxidation of CH_4 as in the cases of CeO_2 and $TbO_{1.75}$ reported by Campbell *et al.* (45). Baronetti *et al.* (94) pointed out that the surface PrO_x species with higher oxidation states (PrO_2 and $PrO_{1.83}$ which contain more Pr^{4+} ions) are active for the formation of CO_x, whereas the more reduced PrO_x species (which contain more Pr^{3+} ions) are responsible for the enhancement in C_{2+} selectivity. Although there are RE^{4+} and RE^{3+} ions in REO_x, the partial substitution of Cl^- ions for RE^{4+} ions to a certain extent would regulate the RE^{4+}/RE^{3+} ratio in the $SrCl_2$-doped REO_x catalysts suitable for the ODE reaction. XPS is a common spectroscopic technique for the determination of the oxidation state of *RE* in REO_x. The *RE* 3*d* or *RE* 4*d* spectra are characterized by complex but distinct features that are related to the final state of the *RE* 4*f* level (53, 56, 95–99). According to the results of XPS studies (Fig. 5), after $SrCl_2$ doping, there is a remarkable increase in RE^{3+} concentrations in the three catalysts. This indicates that the infiltration of $SrCl_2$ into the REO_x lattice enhances the presence of the trivalent *RE* ions. With the rise in H_2 reduction temperature from 500 to 900°C, the RE^{3+} contents augmented, demonstrating that certain amount of RE^{4+} ions had been reduced to RE^{3+}. The color change of the samples during reduction is an indirect evidence for the increase in RE^{3+} content. In other words, the addition of $SrCl_2$ promotes the $RE^{4+} \rightarrow RE^{3+}$ action.

Oxygen Activation and Lattice Oxygen Activity

Previously, we reported the detection of trapped electrons in the SrF_2 (22), $BaCl_2$ (25), $SrCl_2$ (26), or BaF_2 (22, 25, 27)-doped trivalent rare earth oxide (Ln_2O_3) or oxyhalide ($LnOX$) catalysts after treatments in H_2 or

C_2H_6 at a certain temperature; over these catalysts after treatments in O_2, we also detected O^- species. Indeed, on the basis of electroneutrality principle, the intersubstitutions between anionic ions and between cationic ions of alkaline earth halides (MX_2) and rare earth oxides or oxyhalides (with an invariable oxidation state) would cause the generation of trapped electrons in the O–*M*–*X*, O–*Ln*–*X*, *X*–*M*–*Ln*–*X*, and/or O–*M*–*Ln*–*X* species. The activation of oxygen might occur via getting electrons (e_{RE}) that are released in the conversion of RE^{3+} to RE^{4+}:

$$O_2(g) \overset{e_{RE}}{\rightarrow} O_2^-(ads) \overset{e_{RE}}{\rightarrow} O_2^{2-}(ads) \Leftrightarrow 2O^-(ads) \overset{2e_{RE}}{\longrightarrow} 2O^{2-}(ads) \Leftrightarrow 2O^{2-}_{lattice}. \quad [1]$$

For $SrCl_2$-doped REO_x, however, trapped electrons could be generated in the Cl–Sr–*RE*–Cl and O–Sr–*RE*–Cl species. We speculate that, in addition to the above process, the activation of oxygen could also proceed by picking up trapped electrons (e_{trap}):

$$O_2(g) \overset{e_{trap}}{\rightarrow} O_2^-(ads) \overset{e_{trap}}{\rightarrow} O_2^{2-}(ads) \Leftrightarrow 2O^-(ads) \overset{e_{trap}}{\rightarrow} 2O^{2-}(ads) \Leftrightarrow 2O^{2-}_{lattice}. \quad [2]$$

The obvious enhancement in ODE performance over the $SrCl_2$-doped REO_x catalysts might be associated with the combinatory activation of gas-phase oxygen molecules via both pathways [1] and [2].

As observed in the O_2-TPD studies (Fig. 8), desorptions at lower temperatures (600–760°C for CeO_2, 200–500°C for $PrO_{1.83}$, and 300–500°C for $TbO_{1.75}$) were due to surface oxygen adspecies, whereas those at higher temperatures (760–900°C for CeO_2, 600–900°C for $PrO_{1.83}$, and 550–800°C for $TbO_{1.75}$) were due to lattice O^{2-}. Such an assignment was confirmed by the results of O 1*s* XPS studies (Fig. 6). $SrCl_2$ doping lowers the desorption temperatures and increases the extent of lattice oxygen desorption (Figs. 8d–8f), an indication of the enhancements in lattice O^{2-} activity. On the other hand, from the relative intensities of the desorption peaks due to oxygen adspecies (O^-, O_2^{2-}, and/or O_2^-), one can deduce that the addition of $SrCl_2$ has regulated the amounts and distribution of these surface oxygen adspecies, especially on the Ce- and Pr-containing catalysts. During the reduction processes of the catalysts, in addition to the removal of oxygen adspecies, the removal of bulk oxide ions proceeds via either inward diffusion of H_2 from the surface to the bulk or outward diffusion of O^{2-} from the bulk to the surface. Apparently, the activity of lattice O^{2-} and oxygen vacancy density in the catalysts have direct influences on such a reduction process. Harrison *et al.* (100) pointed out that the doping of trivalent cation into a CeO_2 lattice could generate anion vacancies and trivalent cerium ions, leading to an increase in electrical conduction (101). Similarly, the accommodation of Sr^{2+} ions by ionic exchanges in the REO_x lattice would also enhance the electrical conductivity since there are more RE^{3+} ions in the $SrCl_2/REO_x$ catalysts (based on XPS results). It has been revealed that the electrical conductivity of REO_x at high temperatures increases in the order of $CeO_2 < TbO_{1.75} < PrO_{1.83}$ (102), signaling a similar trend for the enhancement in the mobility of lattice O^{2-}. As illustrated in the TPR studies (Fig. 9), the amount of oxygen reducible by H_2 increased with the addition of $SrCl_2$, and the order is 40 mol% $SrCl_2/TbO_{1.75}$ > 30 mol% $SrCl_2/PrO_{1.83}$ > 30 mol% $SrCl_2/CeO_2$ > $PrO_{1.83}$ > $TbO_{1.75}$ > CeO_2. The order for 40 mol% $SrCl_2/TbO_{1.75}$ and 30 mol% $SrCl_2/PrO_{1.83}$ might be associated with the fact that the amount of PrOCl formed in $SrCl_2$-doped $PrO_{1.83}$ is larger than that of TbOCl in $SrCl_2$-doped $TbO_{1.75}$ (Table 3). Long *et al.* (46) reported a similar relative intensity of PrOF and TbOF phases in the XRD investigation of BaF_2-promoted $PrO_{1.83}$ or $TbO_{1.75}$. Furthermore, the doping of $SrCl_2$ lowers the reduction temperatures of lattice oxygen in REO_x (Figs. 9d–9f); this might be related to the formation of defective structures induced in $SrCl_2$ modification. Similar effects have been reported in other doped CeO_2 systems (76, 103–106). In the experiments of C_2H_6-pulsing onto the $^{18}O_2$-treated catalysts, the detection of $H_2{}^{18}O$, ^{18}OH, and ^{18}O demonstrates the involvement of lattice oxygen in the reaction of C_2H_6; the much higher intensities of these species obtained over $SrCl_2$-doped $PrO_{1.83}$ or $TbO_{1.75}$ compared to those over $SrCl_2$-doped CeO_2 are an indication that the activity of lattice oxygen in the former two catalysts is much higher than that in the latter catalyst, coinciding with the sequence of reducibility sequence of the three catalysts. From the results of O 1*s* XPS studies (Fig. 6), one can realize that in addition to lattice O^{2-}, there were O^-, O_2^{2-}, or O_2^- species detected on the catalysts after He treatment at room temperature (Figs. 6Ia–6IIIa and 6Ia′–6IIIa′); but with the increase in H_2 treatment temperature, the oxygen adspecies signals disappeared, indicating that they had reacted with H_2. The generation of O^-, O_2^{2-}, or O_2^- species might be a result of the gaseous O_2 picking up electrons from RE^{3+} ions which are then oxidized to RE^{4+} ions.

As illustrated in the results of *in situ* Raman studies on CeO_2 and 30 mol% $SrCl_2/CeO_2$ (Fig. 7), the addition of $SrCl_2$ noticeably increased the concentrations of O_2^{2-} and O_2^- adspecies [which are generally believed to be active for the selective oxidation of C_2H_6 to C_2H_4 (22–27, 39–41)], indicating that $SrCl_2$ doping promoted O_2 activation over CeO_2. Considering that the defect properties of $SrCl_2/PrO_{1.83}$ and $SrCl_2/TbO_{1.75}$ are similar to that of $SrCl_2/CeO_2$ and their defect densities are considerably higher, it can be inferred that the concentrations of O_2^{2-} and/or O_2^- adspecies on the $SrCl_2$-doped $PrO_{1.83}$ and $TbO_{1.75}$ catalysts are higher than those on $SrCl_2/CeO_2$ and on their undoped counterparts. After $SrCl_2$ doping into $PrO_{1.83}$ and $TbO_{1.75}$, there was a significant decrease in the total amount of oxygen adspecies (O^-, O_2^{2-}, and/or O_2^-) [O_2-TPD (Fig. 8) and TPR

(Fig. 9) studies]; we hence deduce that the relative concentration of O^- adspecies diminished after $SrCl_2$ doping. During oxygen chemisorption, O^- and O_2^- adspecies are usually formed concomitantly and O^- could transform to O_2^{2-}, O_2^-, and/or O^{2-} under certain conditions (107). The reactivity of mono- and polynuclear oxygen species toward light hydrocarbons decreases in the order of $O^- \gg O_2^{2-} > O_2^- > O^{2-}$ (108–113). Due to the highly reactive property, O^- species tend to induce the deep oxidation of ethane and ethene (25, 26, 41, 42). It is clear that besides promoting lattice oxygen activity (thus strengthening the C_2H_6-selective oxidation ability), adding $SrCl_2$ to REO_x increased the concentration of surface oxygen adspecies on 30 mol% $SrCl_2/CeO_2$ (thus improving oxygen activation) and decreased the populations of surface O^- adspecies on 30 mol% $SrCl_2/PrO_{1.83}$ and 40 mol% $SrCl_2/TbO_{1.75}$ (thus reducing C_2H_6 and C_2H_4 deep oxidation reactions). Hence, $SrCl_2$ regulated the surface and bulk properties of REO_x, rendering them suitable for the selective oxidation of C_2H_6 to C_2H_4. As revealed by the data in Table 1 and Fig. 1, the C_2H_4 selectivity followed the order $SrCl_2/TbO_{1.75} > SrCl_2/PrO_{1.83} > SrCl_2/CeO_2$. Taking as well the C_2H_6 conversion into consideration, the catalytic performance followed the sequence of $SrCl_2/TbO_{1.75} > SrCl_2/PrO_{1.83} > SrCl_2/CeO_2$. Therefore, we suggest that O_2^{2-} and O_2^- species are selective for the oxidation of C_2H_6 to C_2H_4, whereas in excessive amount, the O^- species are relatively more active for the deep oxidation of C_2H_6.

CONCLUSIONS

The results show that the doping of $SrCl_2$ to REO_x could noticeably reduce C_2H_4 deep oxidation and hence improve C_2H_4 selectivity and C_2H_6 conversion in ODE reactions. The catalytic performance follows the order of 30 mol% $SrCl_2/CeO_2$ < 30 mol% $SrCl_2/PrO_{1.83}$ < 40 mol% $SrCl_2/TbO_{1.75}$. The leaching of chlorine was modest in the latter two catalysts. However, significant chlorine loss was observed over the first catalyst. Within a period of 60 h on-stream reaction, the $SrCl_2$-promoted $PrO_{1.83}$ and $TbO_{1.75}$ catalysts exhibited stable performance, giving C_2H_6 conversion, C_2H_4 selectivity, and C_2H_4 yield of ca. 79, 71, and 57% for the former and of ca. 83, 76, and 63% for the latter, respectively, at 660°C and 1.67×10^{-4} h g mL^{-1}. From XPS and chemical analyses, it is observed that the Cl^- ions were evenly distributed in 30 mol% $SrCl_2/PrO_{1.83}$ and 40 mol% $SrCl_2/TbO_{1.75}$, whereas that was not the case in 30 mol% $SrCl_2/CeO_2$. XPS investigations on the Ce 3*d*, Pr 3*d*, and Tb 4*d* levels illustrate that RE^{3+} and RE^{4+} ions coexist in the $SrCl_2$-doped catalysts and $SrCl_2$ doping causes the RE^{3+} concentration to increase, promoting interconversion between RE^{3+} and RE^{4+} ions as a result. The results of O_2-TPD and TPR studies reveal that the addition of $SrCl_2$ to REO_x enhances O_2 activation and promotes lattice O^{2-} activity. We believe that these properties are closely related to the defects generated due to interexchange of ions between the $SrCl_2$ and the REO_x phases. From the XRD results, it has been found that, of the three $SrCl_2$-doped catalysts, 40 mol% $SrCl_2/TbO_{1.75}$ possessed a cubic $TbO_{1.75}$ lattice most significantly enlarged and a $SrCl_2$ lattice most pronouncedly shrunk. *In situ* Raman results indicate that there were O_2^{2-} and O_2^- adspecies on the 30 mol% $SrCl_2/CeO_2$ catalyst. O 1*s* XPS studies revealed that there were O^-, O_2^{2-}, and/or O_2^- species over REO_x, 30 mol% $SrCl_2/CeO_2$, 30 mol% $SrCl_2/PrO_{1.83}$, and 40 mol% $SrCl_2/PrO_{1.75}$, with concentrations varied from catalyst to catalyst. On the basis of the results of *in situ* Raman, XPS, O_2-TPD, TPR, and $^{18}O_2$- and C_2H_6-pulsing studies, we suggest that O_2^{2-} and O_2^- as well as surface lattice O^{2-} species are responsible for the selective oxidation of ethane to ethene, whereas in excessive amount, the O^- species are likely to induce the deep oxidation of ethane.

ACKNOWLEDGMENTS

The work described herein was fully supported by a grant from the Research Grants Council of the Hong Kong Special Administration Region, P.R. China (Project No. HKBU 2050/97P). H.X.D. thanks the HKBU for a Ph.D. studentship.

REFERENCES

1. Keller, G. E., and Bhasin, M. M., *J. Catal.* **73**, 9 (1982).
2. Ruth, K., Kieffer, R., and Burch, R., *J. Catal.* **175**, 16 (1998).
3. Ruth, K., Burch, R., and Kieffer, R., *J. Catal.* **175**, 27 (1998).
4. Thorsteinson, E. M., Wilson, T. P., Young, F. G., and Kasai, P. H., *J. Catal.* **52**, 116 (1978).
5. McCain, J. H., U.S. Patent 4 524 236 (1985).
6. Morales, E., and Lunsford, J. H., *J. Catal.* **118**, 255 (1989).
7. Conway, S. J., and Lunsford, J. H., *J. Catal.* **131**, 513 (1991).
8. Wang, D., Rosynek, M. P., and Lunsford, J. H., *J. Catal.* **151**, 155 (1995).
9. Conway, S. J., Wang, D. J., and Lunsford, J. H., *Appl. Catal.* **79**, L1 (1991).
10. Erdöhelyi, A., and Solymosi, F., *J. Catal.* **129**, 497 (1991).
11. Erdöhelyi, A., Máté, F., and Solymosi, F., *J. Catal.* **135**, 563 (1991).
12. Hayakawa, T., Anderson, A. G., Orita, H., Shimizu, M., and Takehira, K., *Catal. Lett.* **16**, 373 (1992).
13. Yi, G., Hayakawa, T., Anderson, A. G., Suzuki, K., Hamakawa, S., York, A. P. E., Shimizu, M., and Takehira, K., *Catal. Lett.* **38**, 189 (1996).
14. Ueda, W., Lin, S. W., and Tohmoto, I., *Catal. Lett.* **44**, 241 (1997).
15. Wang, S. B., Murata, K., Hayakawa, T., Hamakawa, S., and Suzuki, K., *Catal. Lett.* **59**, 173 (1999).
16. Wang, S. B., Murata, K., Hayakawa, T., Hamakawa, S., and Suzuki, K., *Catal. Lett.* **62**, 191 (1999).
17. Sugiyama, S., Sogabe, K., Miyamoto, T., Hayashi, H., and Moffat, J. B., *Catal. Lett.* **42**, 127 (1996).
18. Kennedy, E. M., and Cant, N. W., *Appl. Catal.* **75**, 321 (1991).
19. Bernal, S., Martin, G. A., Moral, P., and Perrichon, V., *Catal. Lett.* **6**, 231 (1990).
20. Ji, L., and Liu, J. S., *J. Chem. Soc., Chem. Commun.* 1203 (1996).
21. Luo, J. Z., and Wan, H. L., *Appl. Catal. A* **158**, 137 (1997).
22. (a) Au, C. T., and Zhou, X. P., *J. Chem. Soc., Faraday Trans.* **92**, 1793 (1996); (b) **93**, 485 (1997).

23. Au, C. T., and Zhou, X. P., *Catal. Lett.* **40**, 101 (1996).
24. Au, C. T., Chen, K. D., Dai, H. X., Liu, Y. W., and Ng, C. F., *Appl. Catal. A* **177**, 185 (1999).
25. Dai, H. X., Liu, Y. W., Ng, C. F., and Au, C. T., *J. Catal.* **187**, 59 (1999).
26. Dai, H. X., Ng, C. F., and Au, C. T., *Appl. Catal. A* **202**, 1 (2000).
27. Au, C. T., Zhou, X. P., Liu, Y. W., Ji, W. J., and Ng, C. F., *J. Catal.* **174**, 153 (1998).
28. Au, C. T., He, H., Lai, S. Y., and Ng, C. F., *J. Catal.* **159**, 280 (1996).
29. Au, C. T., Liu, Y. W., and Ng, C. F., *J. Catal.* **171**, 231 (1997).
30. Au, C. T., Liu, Y. W., and Ng, C. F., *J. Catal.* **176**, 365 (1998).
31. Osada, Y., Koike, S., Fukushima, T., Ogasawara, S., Shikada, T., and Ikariya, T., *Appl. Catal.* **59**, 59 (1990).
32. Kaminsky, M. P., Zajac, G. W., Campuzano, J. C., Faiz, M., Beaulaige, L., Gofron, K., Jenning, G., Yao, J. M., and Saldin, D. K., *J. Catal.* **136**, 16 (1992).
33. Erarslanoglu, Y., Onal, I., Dogu, T., and Senkan, S., *Appl. Catal. A* **145**, 75 (1996).
34. Filkova, D., Wolf, D., Gayko, G., Baerns, M., and Petrov, L., *Appl. Catal. A* **159**, 33 (1997).
35. Gaffney, A. M., Jones, C. A., Leonard, J. J., and Sofranko, J. A., *J. Catal.* **114**, 422 (1988).
36. Poirier, M. G., Breault, R., Kaliaguine, S., and Adnot, A., *Appl. Catal.* **71**, 103 (1991).
37. Yu, Z., Yang, X., Lunsford, J. H., and Rosynek, M. P., *J. Catal.* **154**, 163 (1995).
38. Ito, T., and Lunsford, J. H., *Nature* **314**, 721 (1985).
39. Dissanayake, D., Lunsford, J. H., and Rosynek, M. P., *J. Catal.* **143**, 286 (1993).
40. Mestl, G., Knözinger, H., and Lunsford, J. H., *Ber. Bunsenges. Phys. Chem.* **97**, 319 (1993).
41. Lunsford, J. H., Yang, X., Haller, K., Laane, J., Mestl, G., and Knözinger, H., *J. Phys. Chem.* **97**, 13810 (1993).
42. Hutchings, G. J., Scurrell, M. S., and Woodhous, J. R., *Catal. Today* **4**, 255 (1989).
43. Dubois, J. L., and Cameron, C. J., *Appl. Catal.* **67**, 49 (1990).
44. Otsuka, K., Jinno, K., and Morikawa, A., *Chem. Lett.* 499 (1985).
45. Campbell, K. D., Zhang, H., and Lunsford, J. H., *J. Phys. Chem.* **92**, 750 (1988).
46. Long, R. Q., Luo, J. Z., Chen, M. S., and Wan, H. L., *Appl. Catal. A* **159**, 171 (1997).
47. Long, R. Q., and Wan, H. L., *J. Chem. Soc., Faraday Trans.* **93**, 335 (1997).
48. Long, R. Q., and Wan, H. L., *J. Catal.* **172**, 471 (1997).
49. Tsai, K. R., Chen, D. A., Wan, H. L., Zhang, H. B., Lin, G. D., and Zhang, P. X., *Catal. Today* **51**, 3 (1999).
50. Fujimori, A., *Phys. Rev. B* **28**, 2282 (1983).
51. Fujimori, A., *Phys. Rev. B* **53**, 2518 (1984).
52. Kotani, A., Mizuta, H., Jo, T., and Parlebas, J. C., *Solid State Commun.* **53**, 805 (1985).
53. Wuilloud, E., Delley, B., Schneider, W.-D., and Baer, Y., *Phys. Rev. Lett.* **53**, 202 (1984).
54. Wuilloud, E., Delley, B., Schneider, W.-D., and Baer, Y., *Phys. Rev. Lett.* **53**, 2519 (1984).
55. Jo, T., and Kotani, A., *Phys. Scr.* **35**, 570 (1987).
56. Burroughs, P., Hamnett, A., Orchard, A. F., and Thornton, G., *J. Chem. Soc., Dalton Trans.* 1686 (1976).
57. Matsumura, Y., Sugiyama, S., and Moffat, J. B., *in* "Catalytic Selective Oxidation" (S. T. Oyama and J. W. Hightower, Eds.), ACS Symp. Ser., p. 326, Am. Chem. Soc., Washington, DC, 1993.
58. Sarma, D. D., and Rao, C. N. R., *J. Electron Spectrosc. Relat. Phenom.* **20**, 25 (1980).
59. Sarma, D. D., Hedge, M. S., and Rao, C. N. R., *J. Chem. Soc., Faraday Trans. 2* **77**, 1509 (1981).
60. Ayyoob, M., and Hedge, M. S., *Surf. Sci.* **133**, 516 (1983).
61. Hedge, M. S., and Ayyoob, M., *Surf. Sci.* **173**, L635 (1986).
62. Yamazoe, N., Teraoka, Y., and Seiyama, T., *Chem. Lett.* 1767 (1981).
63. Dubois, J. L., Bisiaux, M., and Mimoun, H., *Catal. Lett.* 967 (1990).
64. Weckhuysen, B. M., Rosynek, M. P., and Lunsford, J. H., *Phys. Chem. Chem. Phys.* **1**, 3157 (1999).
65. Eysel, H. H., and Thym, S., *Z. Anorg. Allg. Chem.* **411**, 97 (1975).
66. Hester, R. E., and Nour, E. M., *J. Raman Spectrosc.* **11**, 64 (1981).
67. Nakamoto, K., Nonaka, Y., Ishiguro, T., Urban, M. W., Suzuki, M., Kozuka, M., Nishida, Y., and Kida, S., *J. Am. Chem. Soc.* **104**, 3386 (1982).
68. Otsuka, K., Yokoyama, S., and Morikawa, A., *Chem. Lett.* 319 (1985).
69. Otsuka, K., Jinno, K., and Morikawa, A., *J. Catal.* **100**, 353 (1986).
70. Otsuka, K., and Komatsu, T., *Chem. Lett.* 483 (1987).
71. Korf, S. J., Roos, J. A., Derksen, J. W. H. C., Vreeman, J. A., van Ommen, J. G., and Ross, J. R. H., *Appl. Catal.* **59**, 259 (1990).
72. Sokolovski, V. D., Buyevskaya, O. V., Plyasova, L. M., Litvak, G. S., and Uvarov, N. Ph., *Catal. Today* **6**, 489 (1990).
73. Maitra, A. M., *Appl. Catal.* **104**, 11 (1993).
74. Au, C. T., Chen, K. D., Dai, H. X., Liu, Y. W., Luo, J. Z., and Ng, C. F., *J. Catal.* **179**, 300 (1998).
75. Trovarelli, A., de Leitenburg, C., and Dolcetti, G., *J. Chem. Soc., Chem. Commun.* 472 (1991).
76. Trovarelli, A., Dolcetti, G., de Leitenburg, C., Kašpar, J., Finetti, P., and Santoni, A., *J. Chem. Soc., Faraday Trans.* **88**, 1311 (1992).
77. Trovarelli, A., Dolcetti, G., de Leitenburg, C., and Kašpar, J., *in* "New Frontiers in Catalysis," p. 2781. Elsevier, Amsterdam, 1993.
78. Asami, K., Kusakabe, K., Ashi, N., and Ohtsuka, Y., *Appl. Catal. A* **156**, 43 (1997).
79. Wang, Y., Takahashi, Y., and Ohtsuka, *J. Catal.* **186**, 160 (1999).
80. Burch, R., Crabb, E. M., Squire, G. D., and Tsang, S. C., *Catal. Lett.* **2**, 249 (1989).
81. Shi, C., Rosynek, M. P., and Lunsford, J. H., *J. Phys. Chem.* **98**, 8371 (1994).
82. Sugiyama, S., Matsumura, Y., and Moffat, J. B., *J. Catal.* **139**, 338 (1993).
83. Bailar, Jr., J. C., Emeleus, H. J., Nyholm, S. R., and Trotman-Dickenson, A. F., Eds., "Comprehensive Inorganic Chemistry," Vol. 4, p. 80. Pergamon, Oxford, 1973.
84. "Handbook of Chemistry and Physics," 72nd ed. CRC Press, Boca Raton, FL, 1991.
85. Brauer, G., and Gingerich, K. A., *J. Inorg. Nucl. Chem.* **16**, 87 (1960).
86. Ray, S. P., Nowick, A. S., and Cox, D. E., *J. Solid State Chem.* **15**, 344 (1975).
87. Perrichon, V., Laachir, A., Bergeret, G., Fréty, R., and Tournayan, L., *J. Chem. Soc., Faraday Trans.* **90**, 773 (1994).
88. Lide, D. R. Ed.,"Handbook of Chemistry and Physics." CRC Press, Boca Raton, FL, 1998–1999.
89. West, A. R., "Solid State Chemistry and its Applications." Courier International Ltd., Great Britain, 1990.
90. Roger, A.-C., Petit, C., Libs, S., and Kiennemann, A., *Stud. Surf. Sci. Catal.* **101**, 1273 (1996).
91. Gschneidner, K. A., Jr., and Erying, L., Eds, "Handbook on the Physics and Chemistry of Rare Earths," Vol. 5, p. 322. North-Holland, Amsterdam, 1982.
92. Eyring, L., *in* "Synthesis of Lanthanide and Actinide Compounds" (G. Meyer and L. R. Morss, Eds.), p. 187. Kluwer Academic, Dordrecht, The Netherlands, 1991.
93. DeBoy, J. M., and Hicks, R. F., *Ind. Eng. Chem. Res.* **27**, 1577 (1988).
94. Baronetti, G. T., Grosso, W. E., Maina, S. P., Padró, C. L., Castro, A. A., Scelza, O. A., and Latasa, J. M. P., *J. Chem. Technol. Biotechnol.* **70**, 141 (1997).
95. Gunnarsson, O., and Schönhammer, K., *Phys. Rev. B* **28**, 4315 (1983).
96. Allen, J. W., *J. Magn. Magn. Mater.* **47/48**, 168 (1985).
97. Kotani, A., Jo, T., and Parlebas, J. C., *Adv. Phys.* **37**, 37 (1988).
98. Romeo, M., Bak, K., El Fallah, J., Le Normand, F., and Hilaire, L., *Surf. Interface Anal.* **20**, 508 (1993).

99. Pfau, A., and Schierbaum, K. D., *Surf. Sci.* **321**, 71 (1994).
100. Harrison, P. G., Creaser, D. A., Wolfindale, B. A., Waugh, K. C., Morris, M. A., and Mackrodt, W. C., *in* "Catalysis and Surface Characterization" (T. J. Dines, C. H. Rochester, and J. Thomson, Eds.), p. 76. Redwood, Melksham, 1992.
101. Gerhardt, R., and Nowick, A. S., *J. Am. Ceram. Soc.* **69**, 641 (1988).
102. Dept. of Metal in Zhongshan University, Ed., "Physics and Chemistry Constants of Rare Earth," p. 51. Metallurgical Industry Publishing House, Beijing, 1978.
103. Barrault, J., Allouche, A., Paul-Boncour, V., Hilaire, L., and Percheron-Guegan, A., *Appl. Catal.* **46**, 269 (1989).
104. Tournayan, L., Marcilio, N. R., and Fréty, R., *Appl. Catal.* **78**, 31 (1991).
105. Bernal, S., Calvino, J. J., Cifredo, G. A., Rodriguez-Izquierdo, J. M., Perrichon, V., and Laachir, A., *J. Catal.* **137**, 1 (1992).
106. Fornasiero, P., Balducci, G., Di Monte, R., Kašpar, J., Sergo, V., Gubitosa, G., Ferrero, A., and Graziani, M., *J. Catal.* **164**, 173 (1996).
107. Bielañski, A., and Haber, J., "Oxygen in Catalysis." Dekker, New York, 1991.
108. Wang, J. X., and Lunsford, J. H., *J. Phys. Chem.* **90**, 5883 (1986).
109. Aika, K., and Lunsford, J. H., *J. Phys. Chem.* **81**, 1393 (1977).
110. Aika, K., and Lunsford, J. H., *J. Phys. Chem.* **82**, 1794 (1978).
111. Takita, Y., and Lunsford, J. H., *J. Phys. Chem.* **83**, 683 (1979).
112. Takita, Y., Iwamoto, M., and Lunsford, J. H., *J. Phys. Chem.* **84**, 3079 (1980).
113. Iwamoto, M., and Lunsford, J. H., *J. Phys. Chem.* **84**, 1710 (1980).